CENTRO DE INVESTIGACION EN MATERIALES AVANZADOS, S. C.

POSGRADO

COMPUTATIONAL STUDY OF THE MOLECULAR DESIGN OF SOME NATURAL DYES AS SENSITIZERS FOR EFFICIENT DSSC

THESIS

TO OBTAIN THE DEGREE OF

Ph.D. in Material Science

By:

M.Sc. Aanuoluwapo Raphael Obasuyi

Thesis Director:

Dra. Norma Rosario Flores Holguín

CHIHUAHUA, CHIH:, MEXICO **FEBRUARY, 2020**

ACKNOWLEDGMENTS

Above all, I would like to thank the Almighty God for the sound health and strength He provided throughout this program.

I am very thankful to my supervisor, Dra. Norma Rosario Flores Holguín, for the constant support, suggestions and motivation that I received from her during the period of my PhD work. I have been extremely lucky to have a supervisor who cared so much about my work, and who responded to my questions and queries so promptly. Your guidance is deeply appreciated. I appreciate the guidance of my research committee: Dr. Daniel Glossman-Mitnik, Dr. Erasmo Orrantia, Dr. Ricardo Beltrán and Dra Luz Maria Rodriguez Valdez for all your time, patience, guidance, encouragement, outstanding hard work, and for always being there when I needed you.

To my immediate, extended family and friends, for their encouragement and support: Firstly, to my wife Ngozi, for all the love, encouragement and the support you gave. My daughter Oluwapemisire, you are the reason I worked so hard. Thank you for the understanding when I was unable to spend time with you. I love you! To my parents, my brothers for their belief in me and always inspiring me to greater things!

My gratitude also goes to my lab mates, Hugo, Linda and Kathy, my friends: kalu, Mhydeen, Emmanuel and glory for their advice and support. I cannot but appreciate Dr B.J Falaye for showing me the path.

I would like to extend my gratitude to CONACYT for providing the scholarship grant for my program, to CIMAV and everyone, space cannot permit me to be mentioning names, you are awesome. I would like to thank once again all the people who helped me in one way or another for the successful completion of my research work.

TABLE OF CONTENTS

LIST OF FIGURES

LIST OF TABLES

LIST OF ABBREVIATIONS

ΔG_{inject}:	Driving force of electron injection
ΔG_{reg}:	Reorganization energy
D-π-A:	Donor-Bridge-Acceptor
DFT:	Density functional theory
DSSC:	Dye sensitized solar cells
fs:	femto
HF:	Hartree fock
HOMO:	Highest occupied molecular orbital
LHE:	Light-Harvesting Efficiency
LUMO:	Lowest unoccupied molecular orbital
N3:	cis-dithiocyanatobis-(4,4′-dicarboxy-2,2′-bipyridine) ruthenium(II)
NIR:	Near Infra-red
ps:	picosecond
SnO_2:	Tin(IV) oxide
TD-DFT:	Time dependent Density functional theory
TiO_2:	Titanium dioxide
V_{oc}:	Open circuit voltage
V_{RP}:	electronic coupling between the reactants and products
ZnO:	Zinc Oxide

I. ABSTRACT

The global energy consumption is expected to double by 2050. The excessive use of fossil fuels which is a main source of energy generation has resulted in a serious environmental issues such as global warming. There is great demand for replacing fossil fuels with clean, renewable and sustainable energy sources such as solar energy. Dye sensitized solar cells (DSSC) are type of solar cells which has gained considerable attention in the last two decades. , However, their efficiencies are still lower than the traditional solar cells. A considerable and increasing amount of research efforts have been devoted to design and synthesis new materials such as dye sensitizers as a route to improve DSSC's power conversion efficiency. This drawback calls for applying new methods such as computational modelling and rational designing of new materials.

In this research, selected members of the anthocyanidin and betalain families were carefully studied and the electron transfer properties of these molecules were compared. These dyes families have been successfully proven to show high conversion efficiency in DSSC devices because both molecules possess hole-transporting ability. Considering this ability, their electron inject properties must be well known and some molecular arrangement are desirable to improve this characteristics.

A theoretical investigation was carried out using density functional theory at the MN12SX/6-311+G(d,p) level of theory which was decided after a validation from four different functionals, to calculate and compare the photoinduced electron injection for selected members of the anthocyanidin and betalain families. The rate constant of the injection for both families was calculated, and it was verified that the regeneration in the dye

during the DSSC operation is caused by an energetic electron injection of the matched electrons in the dye.

Two modifications of the molecular structures of Aurantinidin and Betanidin dyes were done and the optical and electrical properties were calculated by using density functional theory (DFT) and time-dependent DFT (TD-DFT). Modification of the structures was done adding units connected by vinyl and using regular electron acceptor and electron donor moieties to the original structure. A further modification using the donor-bridge-acceptor model was done on Aurantinidin. The modifications improved the electron injection of the molecules with high light harvesting efficiency (LHE), driving force of electron injection (ΔG_{inject}), reorganization energy (ΔG_{reg}) and open-circuit photovoltage (V_{OC}).

The present research shows that the rate constant of electron injection of the dyes are good enough to enhance electron movement for improve DSSC efficiency. A prediction of the best dye based on the above properties was made for the maximum efficiency of the DSSC to be achieved.

Keywords: DSSC, Electron Injection, Anthocyanidin, Betalain

II. RESUME

Se espera que el consumo mundial de energía se duplique para el año 2050. El uso excesivo de combustibles fósiles, que es una fuente principal de generación de energía, ha dado lugar a graves problemas ambientales como el calentamiento global. Existe una gran necesidad para reemplazar los combustibles fósiles con fuentes de energía limpias, renovables y sostenibles, como la energía solar. Las celdas solares sensibilizadas con colorante (DSSC) son un tipo de celdas solares que han ganado considerable atención en las últimas dos décadas. Sin embargo, sus eficiencias son aún más bajas que las celdas solares tradicionales. Se han dedicado una cantidad considerable y creciente de investigaciones al diseño y síntesis de nuevos materiales, como los sensibilizadores al colorante, como una ruta para mejorar la eficiencia de conversión de la potencia en las DSSC. Este inconveniente requiere la aplicación de nuevos métodos como el modelado computacional y el diseño racional de nuevos materiales.

En esta investigación, los miembros seleccionados de las familias de antocianidina y betalaína se estudiaron cuidadosamente y se compararon las propiedades de transferencia de electrones de estas moléculas. Se ha demostrado con éxito que estas familias de tintes muestran una alta eficiencia de conversión en dispositivos DSSC porque ambas moléculas poseen la capacidad de transportar huecos. Teniendo en cuenta esta capacidad, sus propiedades de inyección de electrones deben ser bien conocidas y algunos arreglos moleculares son deseables para mejorar estas características.

Se llevó a cabo una investigación teórica utilizando la Teoría de Funcionales de la Densidad con el nivel de teoría MN12SX / 6-311+G (d, p) que se decidió después de una validación de cuatro funcionales diferentes, para calcular y comparar la inyección de

electrones fotoinducida para miembros seleccionados de las familias antocianidina y betalaína. Se calculó la constante de velocidad de inyección para ambas familias, y se verificó que la regeneración en el tinte durante la operación de la DSSC es causada por una inyección energética de electrones de los electrones emparejados en el tinte.

Se realizaron dos modificaciones de las estructuras moleculares de los colorantes Aurantinidin y Betanidin y se calcularon las propiedades ópticas y eléctricas utilizando la Teoría de Funcionales de la Densidad (DFT) y DFT dependiente del tiempo (TD-DFT). La modificación de las estructuras se realizó agregando unidades conectadas por vinilo y utilizando aceptores de electrones regulares y estos donadores de electrones a la estructura original. Se realizó una modificación adicional utilizando el modelo donante-puente-aceptor en Aurantinidin. Las modificaciones mejoraron la inyección de electrones de las moléculas con alta eficiencia de captación de luz (LHE), fuerza impulsora de la inyección de electrones (ΔG_{inject}), energía de reorganización (ΔG_{reg}) y fotovoltaje de circuito abierto (V_{OC}).

La presente investigación muestra que la constante de la velocidad de inyección electrónica de los colorantes es lo suficientemente buena como para mejorar el flujo de electrones para aumentar la eficiencia en las DSSC. Se realizó una predicción del mejor tinte en base a las propiedades anteriores para lograr la máxima eficiencia de las DSSC.

Palabras clave: DSSC, inyección electrónica, antocianidina, betalaína

III. INTRODUCTION

Dye-sensitized solar cells (DSSCs) show great potential as low-carbon sources of energy, Dye-sensitized solar cells (DSSCs) are attractive solar energy production because they are made from cheap materials that do not need to be highly purified and can be printed at low cost[1–7]. DSSCs are unique compared with almost all other kinds of solar cells in electron transport, light absorption and hole transport that are each handled by different materials in the cell[1]. The sensitizing dye in a DSSC is anchored to a wide-bandgap semiconductor such as Titanium dioxide (TiO_2), Tin(IV) oxide (SnO_2) or Zinc Oxide (ZnO)[8]. The dye plays a vital role during absorption of light by which the excited electrons are injected into the semiconductor conduction band and travel to reach the counter-electrode[9]. When the dye absorbs light, the photoexcited electron rapidly transfers to the conduction band of the semiconductor, which carries the electron to one of the electrodes[10].

To achieve highly efficient DSSC, there are some requirements for the sensitizers:

(a) wide absorption ranges for the whole visible and near-infrared regions,

(b) high molar absorption coefficients,

(c) lowest unoccupied molecular orbital (LUMO) energy level should be above the conduction band edge of the semiconductor to be used with electrons localized near the anchoring group for efficient electron injection,

(d) highest occupied molecular orbital (HOMO) energy level should be below the redox mediator for efficient electron reduction in dye regeneration,

(e) No aggregation on the semiconductor surface.

(f) For a good photocurrent response, the light-harvesting ability of the dye must be high.

(g) For a high photoinduced intramolecular charge transfer, the conjugation between the donor and anchoring group must be intact[8, 11–14].

There has been great progress in the materials composition of DSSC devices not only to enhance device efficiency but also to improve stability and processability and to reduce production costs[15]. Great progress has been made at understanding the science of the processes underlying device performance and it is an interesting starting point to assess the influence of shifting the surface potential of the oxide on device performance and to test whether this can give a further increase in efficiency for our hypothetically optimized devices[16].

Almost all the organic sensitizers applied in DSSCs have three important parts:

1) the electron donor,
2) the electron acceptor, and
3) the linker units for the pi conjugation to enhance the molar absorption coefficient[17].

Injection of electrons from the dye into the semiconductor typically happens on a femto(fs)-to picosecond(ps) time scale whereas charge recombination occurs in the micro to millisecond time scale[18]. The rate constant for injection of electron is on a time scale < 100 fs[19]. The rate is comparable to the rate of intramolecular energy redistribution[19]. The time scale is important because this gives us the range at which the charge transfer or resulting electron injection can cover.

The roadmaps for intramolecular charge transfer and the resulting electron transfer has been theoretically investigated by a lot of quantum chemical techniques, these techniques

are very useful tool due to their efficiency for the interpretation of experimental data[20, 21]. Quantum chemical techniques has shown the importance carried by the electronic coupling between the reactants and products (V_{RP}) in the simplification of electron transfer reactions. Time-dependent density functional theory (TDDFT) is one of the frequently used approaches for calculating electronic excited states; it normally gives results that agree with experimental data at low computational costs, most especially when hybrid functionals are used[9, 10, 22–29]. We reported the theoretical study of anthocyanidin and betalain family dyes.

In this research, it was hypothesized that a good sensitizer molecule for DSSC which has one and/or two carboxyl anchoring groups needs to absorb in the NIR (near Infra-red) for a better light harvesting. Also, the presence of hydroxyl groups in the sensitizer would be beneficial to prevent dye aggregation. Anthocyanidin family considered in this research are Aurantinidin, Cynadin, Delphinidin, and Pelargonidin while Betanidin, Isobetanidin, Indicaxanthin, and Portulaxanthin were considered from the betalains family. These dyes were selected because they are the most common anthocyanidins and betalains found in edible plants that we consume on a daily basis[30]. DFT calculations were done using functionals like B3LYP, M06, M06L and MN12SX with basis set 6-311+G(d,p) during validation, Furthermore, we used TD-DFT calculations to investigate the electronic absorption spectra in the gas and solvent phases during validation.

In this work, further analysis of the molecular arrangements of Anthocyanidin and Betalain family using Aurantinidin and Betanidin respectively as a case study because both showed a better electron injection from the selected members of the families. We further modified the structure by connecting two units of a molecule with a vinyl and a Rhodanine-3-acetic acid added as the electron acceptor. Also, a Donor-Bridge-Acceptor (D-π-A) format

modifications was done where diphenylamine and triphenylamine are used as donor moiety and acrylic acid and phenyl-cyanoacrylic acid used as acceptor moiety.

3.1 JUSTIFICATION

Solar energy is expected to be a good candidate for a future renewable energy source. The energy provided by the sun in one hour is larger than the energy consumption globally in an entire year. However, capturing solar energy and converting it to chemical or electrical energy with a low cost is still a big challenge.

Since 1991, dye-sensitized solar cells (DSSCs) have been extensively studied as an alternative to silicon-based solar cells, owing to their simple structure, transparency, flexibility, low production cost, and wide range of application. Despite these advantages, the low efficiency of DSSCs compared to that of silicon-based cells has limited their commercial implementation[31, 32]. Consequently, there is a critical need to improve the efficiency of state-of-the-art DSSCs in order to realize next-generation solar cells[32].

In order to improve the efficiency of DSSC, there is a quick need for the computation and comparison of the molecular design structure of sensitizers used in making DSSC, in this regard, this study will implement the theoretical background of some types of sensitizers that will be used.

3.2 HYPOTHESIS

The efficiency of anthocyanidin and betalain based DSSC can be improved with the modification of the structure which will bring about efficient electron injection into the semiconductor materials.

3.3 GENERAL OBJECTIVE

To carry out the theoretical study of the structure, electronic properties and electron injection of the anthocyanidin family and betalain dyes and to optimize their sensibility performance, using the Density Functional Theory (DFT).

3.4 SPECIFIC OBJECTIVES

1. The purpose of this study is to compute some selected Anthocyanin and Betalain families for efficient DSSC using different basic sets and functionals.
2. To analyze the HOMO-LUMO configuration of the natural dyes for a better prediction.
3. To analyze the Light-Harvesting Efficiency (LHE) and predict a better efficiency with the use of sensitizers adopted for consideration.
4. To modify the structure of Anthocyanidin and Betalain families in an attempt to improve electron injection.

IV. LITERATURE REVIEW

Zhiang Wang *et al* (2016)[33] did a step-by-step theoretical protocol based on the density functional theory (DFT) and time-dependent DFT (TD-DFT). The study was performed on a Ruthenium polypyridyl complex named cis-dithiocyanatobis-(4,4′-dicarboxy-2,2′-bipyridine) ruthenium(II) (N3), to sensitized TiO_2 solar cell including dye excitations and electronic injection. They investigated the optical absorption spectra of N3 and the complexes of N3-TiO_2 by means of TD-DFT with different DFT XC functionals. Obvious charge transfer characteristics has been visualized in low-lying dipole-allowed excited states, and using TD-PBE0-1/3 functional, they achieved a satisfied consistent with the experimentally-measured spectra and gotten insights into charge transfer character of the lower-lying electronic transitions. They showed the adsorption geometries of N3 anchored on $(TiO_2)_{38}$ nanoparticle, the effects of absorption manners on UV–visible absorption spectroscopes, the energy alignment of molecular levels with respect to the substrate band edges, and the electronic injection pathways as well. With the analysis of different anchoring modes, the electronic structures and excited states of dye-TiO_2 complexes, they suggested the possible pathways of electron injection for the different anchoring modes. The overall picture extracted from their work indicates an important role of the dye adsorption energy and geometry on the electrochemical properties and the DSSC efficiency. This calculation provides a detailed theoretical understanding of the interactions between the sensitizer and the substrate, and gets insight into the effect of the DFT XC functionals and solvent. It is an important step toward optimization of computational details in the later theoretical calculation.

Nora-Aydee *et al* (2015)[34] studied seven functionals (M06-L, M06, M06-2X, M06-HF, M11, PBE0 and B3LYP) with two different basis set (6-31G(d) and 6-31+G(d,p)) for geometry optimization after a semiempirical conformational analysis and for the excited state calculation. This was used in the determination of the absorption spectrum in two chemical arrangements, Cyanidin (Cy) and Cyanidin-chloride (Cy-Cl). Cyanidin-chloride arrangement was studied trying to reproduce the ethanol/HCl environment of the experimental results. They found that functionals with minor Hartree–Fock exchange amount exhibit a better correlation to the experimental value for the electronic absorption properties of the Cy molecule. The calculated vertical excitation energies were affected by the Hartree–Fock exchange involved in the exchange– correlation functional, they recommend B3LYP functional to optimize the geometry and the M06-L as the optimum functional to find the maximum absorption wavelength for this kind of structures. The basis set effect is not significant to the equilibrium structure determination nor to the absorption wavelength definition.

Frau *et al* (2017)[35] reported the assessment of the Minnesota family of density functionals, their usefulness and the molecular systems structure consisting of three citrus flavonoids molecules with potential to inhibit the nonenzymatic glycation of amino acids and proteins and considered antioxidants for avoiding the action of metal Fe. Conceptual DFT is used in calculating the chemical reactivity descriptors and active sites for nucleophilic and electrophilic attacks chosen by linking them to Fukui function indices, the condensed local hypersoftness (LHS) and the dual descriptor. The accuracy of the studied density functionals alongside their validity is checked by comparing their results in descriptors calculated using vertical energy values with the HOMO and LUMO results derived from Koopmans' theorem

approximation. The study tested a Minnesota group of density functionals on whether they accomplish the Koopmans' theorem in DFT through comparison of HOMO- and LUMO-generated values against those derived through the ΔSCF procedure. As per the results, the range-separated, hybrid MN12SX as well as the range-separated, hybrid N12SX optimally meet the objective being tested. Consequently, they confirm as a good alternative to use in place of density functionals reported to showing tuned signs through gap-fitting procedure. This illustrates their usefulness in describing chemical reactivity of large-sized molecular systems.

Muthaiyan Lakshmanakumar et *al* (2018)[36] studied the computational analysis of flavylium compound which consists of anthocyanin pigments: callistephin, Chrysanthemum, oenin and mytrillin, and anthocyanidin pigments: peonidin and petunidin dyes which are used to identify the potential photosensitizer for dye-sensitized solar cell (DSSC). They used Density functional theory to study methoxyl and hydroxyl groups in the pigments. The computed results of six dyes show good oscillator strength (f), light-harvesting efficiency, electron injection and electron regeneration. The short-circuit current density (J_{sc}), total reorganization energy (λ_{total}) and open-circuit voltage (V_{oc}) were also analyzed, dye with smaller reorganization energy has a tendency for high efficiency.

Alessandro Sinopoli *et al* (2017)[37] studied five naturally most abundant anthocyanidins (delphinidin, cyanidin, pelargonidin, malvidin, and peonidin) experimentally and theoretically for dye-sensitized solar cell (DSSC) applications. The five dyes were characterized by UV–Vis absorption spectroscopy and cyclic voltammetry, revealing ideal photophysical and electrochemical properties for their final DSSC application. The molecular geometries, electronic structures, vertical transitions and proton affinity of these

molecules were investigated with DFT and TDDFT calculations. All of the studied dyes show photo-energy conversion activity, with efficiencies up to $\eta = 1.4\%$ for pelargonidin. Computational calculations were fundamental tools in order to better understand the chemical and photophysical properties of the studied dyes. In particular, the molecular orbital analysis shows a correct HOMO and LUMO position and delocalization for efficient electron injection and dye regeneration. PCM-TDDFT results show that the dominant electronic transition of all five natural dyes is from HOMO to LUMO. The experimental and theoretical results in this work dispel the myth of Cyanidin as, so far considered, the most efficient Anthocyanidin dye and they also call into question the catechol chelating binding reputed to be the ideal anchoring mode for Anthocyanidin dyes. Despite these dyes not being novel within the DSSC field, this study links together all the chemical and photophysical aspects which characterise a dye and determine its photo-energy conversion efficiency.

Fritz J. Knorr *et al* (2015)[38] reported spectroelectrochemical and transient absorption spectroscopic studies of electron injection from the plant pigment betanin (Bt) to nanocrystalline TiO_2. Spectroelectrochemical experiments and density functional theory (DFT) calculations are used to interpret transient absorption data in terms of excited state absorption of Bt and ground-state absorption of oxidation intermediates and products. Comparison of the amplitudes of transient signals of Bt on TiO_2 and on ZrO_2, for which no electron injection takes place, reveals the signature of two-electron injection from electronically excited Bt to TiO_2. Transient signals observed for Bt on TiO_2 (in contrast to ZrO_2) on the nanosecond time scale reveal the spectral signatures of photo-oxidation products of Bt absorbing in the red and the blue. These are assigned to a one-electron oxidation product formed by recombination of injected electrons with the two-electron oxidation product. They

concluded that electron injection is a simultaneous two-electron process, recombination is a one-electron process. The formation of a semiquinone radical through recombination limits the efficiency and long-term stability of the Bt-based dye-sensitized solar cell. Strategies are suggested for enhancing photocurrents of dye-sensitized solar cells by harnessing the two-electron oxidation of organic dye sensitizers.

Eka Cahya Prima *et al* (2016)[39] reported that Anthocyanin natural dye was used as a good photosensitizer for TiO_2 solar cells due to its availability as well as its performance. However, the dye still has a problem regarding its narrow absorbance at 550 nm. The increased the dye's absorbance up to NIR spectrum so that it will increase the TiO_2 solar cell performance. The cyanidin-3-glucoside-7- diphenilamine-2'-acrylic acid (CGDA) was used as the new modification of D-π-A functional material in anthocyanin dye. The investigation of the material was carried out by the density functional theory of TD-DFT/UB3LYP/6-31+G(d,p) level. The findings show that first; the dye absorbance has broadened up to 885 nm due to the reduction of gap energy and the increase of electronic transition probabilities from 84.7% to 96.0%. Second, the molecular orbital analysis shows that both diphenylamine and acrylic acid perform as promising donor and acceptor groups for anthocyanin. Third, CGDA has a light-harvesting efficiency of 46.7% surrounding the NIR spectrum area. Finally, the NIR anthocyanin dye possessing HOMO of -5.536 eV and LUMO of -2.886 eV fulfills the criteria of both the effective charge transfer from LUMO dye into conduction band TiO_2 and the good dye regeneration by the electrolyte redox.

Ryuzi Katoh (2012)[40] studied the efficiency of electron injection in dye-sensitized nanocrystalline films through transient absorption (TA) and time-resolved microwave conductivity (TRMC) measurements. They showed the absolute value of electron injection

for several dye-sensitized nanocrystalline films and discuss the relationship between electron injection and the free energy change ($-\Delta G_{inj}$) for the injection process. Some systems exhibited lower electron injection values even when $-\Delta G_{inj}$ was sufficiently large to promote electron injection. There Quantitative evaluation of electron injection using TA and TRMC gives new insights for developing high-performance solar cell devices.

S. Akın *et al* (2016)[41] reported that nine different natural dyes having various anchoring groups were extracted from various plants and used as photo-sensitizers in DSSC applications. They obtained an electron injection kinetics by the cyclic voltammetry observations and are in good agreement with the results obtained by the photoinduced electron transfer analysis. Their results show that Anthocyanin dye has the most appropriate LUMO level for rapid electron injection. The DSSC sensitized by long-hydroxyl & carbonyl-chain bearing (the combination of carbonyl and hydroxyl as anchoring groups) anthocyanin, offered the best PCE of 1.87% among the nine extracts due to its higher electron injection rate (k_{ET}). However, the PCE is still lower by a factor of 4–5 compared with Ru based synthetic dyes. Nonetheless, natural dyes are quite useful for their non-poisonity, and very low cost of production opening up a perspective of feasibility for economic and environmentally friendly dye cells. Therefore, natural dyes as light harvesting elements in DSSCs can contribute to a sustainable solution in future energy production.

Julien Preat (2010)[42] did a theoretical investigation to model the mechanisms of photoinduced electron injection and energy transfer for a recent organic metal-free dye derived from the triphenylamine (2TPA-R) structure. The 2TPA-R system results from the fusion between two TPA moieties connected by a vinyl group, and the rhodanine-3-acetic acid is used as the electron acceptor group. DFT and TDDFT approaches have been exploited

to calculate the key parameters controlling the intramolecular charge transfer (ICT) injection and transfer rate constants in the classical Marcus formalism: (i) the electronic coupling; (ii) the reorganization energies; and (iii) the variation of the Gibbs energy. They managed not only to gain insights into the geometrical and electronic structures of triphenylamine (2TPA-R) organic dyes but also to bring out the adequate structural modifications optimizing the properties of the TPA-based DSSCs. In particular, DFT and TDDFT approaches have been exploited to calculate the key parameters controlling the intramolecular charge transfer (ICT) injection and transfer rate constants in the classical Marcus theory. In complete agreement with the experimental trends, they showed (i) two excited states calculated at 2.78 and 3.33 eV, (ii) the energy transfer (ET) between these two states is in competition with the electron injection from the excited state; (iii) they clearly underlined that the standard Marcus model is certainly unsuitable to delivers realistic rate constants for electron injections at high potential; (iv) the use of a square root model helps to calculate valuable injection time scales.

Results and methodologies from different authors highlighted above were considered and helped to design this research. Conducting a proper validation process, defining the molecular systems families and thereafter calculating the electronic properties of the molecules and developed modification of the structures. All this concepts helps us to be able to design a system that will be useful to get a better and more efficient electron injection for a DSSC.

V. THEORETICAL BACKGROUND

5.1 COMPUTATIONAL CHEMISTRY

Computational chemistry is an exciting and fast-emerging discipline which deals with the modeling and the computer simulation of systems such as biomolecules, polymers, drugs, inorganic and organic molecules. Since its advent, computational chemistry has grown to the state it is today and it became popular being immensely benefited from the tremendous improvements in computer hardware and software during the last several decades. With high computing power using parallel or grid computing facilities and with faster and efficient numerical algorithms, computational chemistry can be very effectively used to solve complex chemical and biological problems[43].

Software tools for computational chemistry are often based on empirical information. To use these tools effectively it is necessary to understand the method of implementation of this technique and the nature of the database used in the parameterization of the method. Then, it is possible to redesign the tools for specific investigations and define the limits of confidence in results. In the real modeling procedure of a system, it must be noted the natural criteria associated with the formation of that system and incorporate all these factors to make the model close to the natural system. All-natural processes are associated with at least one of the following criteria:[43]

1. An increase in stability: Stability is a very broad term comprising structural stability, energy stability, potential stability, and so on. During modeling, the thermodynamic significance (energetics) of stability, is to make the energy of the system as low as possible.

2. Symmetry: Nature likes symmetry and dislikes identity. To be more precise, we can say that in nature no two materials are identical, but they may be symmetrical.
3. Quantization: This term stands for fixation. For a stable system, everything is quantized. Properties, qualities, quantities, influences, etc. are quantized.
4. Homogeneity: A number of natural processes are there such as diffusion, dissolution, etc., which are associated with the reallocation of particles in a homogeneous manner.

5.1.1 Semi-empirical Calculations

Semiempirical methods of quantum chemistry start out from the ab initio formalism and then introduce assumptions to speed up the calculations, typically neglecting many of the less important terms in the ab initio equations. In order to compensate for the errors caused by these approximations, empirical parameters are incorporated into the formalism and calibrated against reliable experimental or theoretical reference data. It is generally recognized that ab initio methods and even DFT can give the right result for the right reason, not only in principle, but often in practice, and that semiempirical calculations can offer qualitatively correct results of useful accuracy for many larger and chemically interesting systems. Semiempirical calculations are usually faster than DFT computations by more than two orders of magnitude, and therefore they often remain the method of choice in applications that involve really large molecules (biochemistry) or a large number of molecules or a large number of calculations (dynamics). Today, many chemical problems are solved by the combined use of ab initio, DFT, and semiempirical methods.[44]

5.1.2 Ab Initio Calculations

Ab initio means “from the beginning” or “from first principles”. Ab initio quantum chemistry distinguishes itself from other computational methods in that it is based solely on established laws of nature: quantum mechanics. Over the last two decades powerful molecular modelling tools have been developed which are capable of accurately predicting structures, energetics, reactivity and other properties of molecules. These developments have come about largely due to: The dramatic increase in computer speed. The design of efficient quantum chemical algorithms.[45]

5.1.3 Density Functional Theory (DFT)

Density functional theory (DFT) is a quantum mechanical theory used in physics and chemistry to investigate the electronic structure (principally the ground state) of many-body systems, in particular atoms, molecules, and the condensed phases. With this theory, the properties of a many-electron system can be determined by using functionals, i.e. functions of another function, which in this case is the electron density. The multiple determinant calculations require very large basis sets due to the poor convergence of the correlation energy when the inter-electronic distance becomes very small. However, DFT can produce accurate results with relatively small basis sets. DFT has become the most popular and versatile method in computational chemistry, accounting for approximately 90% of all calculations today. The reason for this preference is that DFT scales with the same order as HF theory ($N3$, where N is proportional to system size). DFT avoids the expense of the more traditional methods, deriving the energy directly from the electron probability density, rather than the molecular wavefunction, thus drastically reducing the dimensionality of the

problem. Regardless of how many electrons one has in the system, the density is always 3 dimensional.[46]

Different functionals and methods used in DFT computations are as follows:

- Electron Density
- Pair Density
- The Hohenberg-Kohn theorems
- The uniform electron gas
- The non-uniform electron gas
- Kohn-Sham DFT
- Local-density approximation
- Generalized gradient approximation
- The hybrid functionals
- The meta-GGAs

5.2 BASIS SETS

The atom-centred functions used to describe the atomic orbitals are known as basis functions and collectively form a basis set Larger basis sets give a better approximation to the atomic orbitals as the place fewer restrictions on the wavefunction Larger basis sets attract a higher computational cost Basis sets are carefully designed to give the best description for the lowest cost

5.2.1 Classification of Basis Sets

Basis set can be broadly classified into the following types[47].

1. Minimal basis sets: STO-3G, STO-4G, STO-6G, STO-3G*
2. Pople basis sets: 3-21g, 3-21g* – Polarized, 3-21+g – Diffuse, 3-21+g* – With polarization and diffuse functions, 6-31g, 6-31g*, 6-31+g*, 6-31g (3df, 3pd),6- 311g, 6-311g*, 6-311+g*.
3. Correlation consistent basis sets: Examples of these are cc-pVDZ (correlation consistent valence double zeta) cc-pVTZ (correlation consistent valence triple zeta) cc-pVQZ (correlation consistent valence quadruple zeta), cc-pV5Z (correlation consistent valence quintuple zeta), aug-cc-pVDZ (Augmented versions of cc-pVDZ), etc.
4. Other split valence basis sets: (They have generic names), such as SV(P), SVP, DZV, TZV, TZVPP, or valence triple-zeta plus polarization, QZVPP, valence quadruple-zeta plus polarization.
5. Double, triple, and quadruple zeta basis sets: The most common is the D95 basis set of Dunning.
6. Plane-wave basis sets: In addition to localized basis sets, plane-wave basis sets can also be used in quantum chemical simulations. Typically, a finite number of plane wavefunctions are used, below a specific cutoff energy which is chosen for a certain calculation.

5.3 QUANTUM MECHANICS: A BRIEF INTRODUCTION

The postulates and theorems of quantum mechanics form the rigorous foundation for the prediction of observable chemical properties from first principles[48]. Expressed somewhat loosely, the fundamental postulates of quantum mechanics assert that microscopic systems are described by ‘wave functions’ that completely characterize all of the physical

properties of the system. In particular, there are quantum mechanical 'operators' corresponding to each physical observable that, when applied to the wave function, allow one to predict the probability of finding the system to exhibit a particular value or range of values (scalar, vector, etc.) for that observable.

However, many successful chemical models exist that do not necessarily have obvious connections with quantum mechanics. Typically, these models were developed based on intuitive concepts, i.e., their forms were determined inductively. In principle, any successful model *must* ultimately find its basis in quantum mechanics, and indeed *a posteriori* derivations have illustrated this point in select instances, but often the form of a good model is more readily grasped when rationalized on the basis of intuitive chemical concepts rather than on the basis of quantum mechanics (the latter being desperately non-intuitive at first blush)[48].

5.3.1 The Time-Independent Schrödinger Equation

The famous time-independent Schrödinger equation:

$$\frac{d^2\psi(x)}{dx^2} + \frac{2m}{\hbar^2}\left|E - V(x)\right|\psi(x) = 0 \tag{5.1}$$

which is almost always written in the form:

$$-\frac{\hbar^2}{2m}\frac{d^2\psi(x)}{dx^2} + V(x)\psi(x) = E\psi(x) \tag{5.2}$$

This single-particle one-dimensional equation can easily be extended to the case of three dimensions, where it becomes:

$$-\frac{\hbar^2}{2m}\nabla^2\psi(r)+V(r)\psi(r)=E\psi(r) \tag{5.3}$$

A two-body problem can also be treated by this equation if the mass m is replaced with a reduced mass.

5.3.2 The Time-Dependent Schrödinger Equation

The time-dependent Schrödinger equation cannot be derived using elementary methods and is generally given as a postulate of quantum mechanics. The single-particle three dimensional time-dependent Schrödinger equation is:

$$i\hbar\frac{\partial\psi(r,t)}{\partial t}=-\frac{\hbar^2}{2m}\nabla^2\psi(r,t)+V(r)\psi(r,t) \tag{5.4}$$

If we write the wavefunction as a product of spatial and temporal terms, $\psi(r,t)=\psi(r)\,f(t)$ then equation 5.4 becomes

$$\psi(r)i\hbar\frac{\partial f(t)}{\partial t}=f(t)\left[-\frac{\hbar^2}{2m}\nabla^2+V(r)\right]\psi(r) \tag{5.5}$$

$$\text{or : }\frac{i\hbar}{f(t)}\frac{\partial f(t)}{\partial t}=\frac{1}{\psi(r)}\left[-\frac{\hbar^2}{2m}\nabla^2+V(r)\right]\psi(r) \tag{5.6}$$

Since the left-hand side is a function of t only and the right-hand side is a function of r only, the two sides must equal a constant. If we tentatively designate this constant E (since the right-hand side clearly must have the dimensions of energy), then we extract two ordinary differential equations, namely:

$$\frac{1}{f(t)}\frac{\partial f(t)}{\partial t} = -\frac{iE}{\hbar} \tag{5.7}$$

And

$$\left[-\frac{\hbar^2}{2m}\nabla^2\psi(r) + V(r)\psi(r)\right] = E\psi(r) \tag{5.8}$$

$$\left[-\frac{\hbar^2}{2m}\nabla^2 + V(r)\right]\psi(r) = E\psi(r) \tag{5.9}$$

Where the term in square bracket on the LHS is called the Hamiltonian operator. The latter equation is once again the time-independent Schrödinger equation. The former equation is easily solved to yield:

$$f(t) = e^{-iEt/\hbar} \tag{5.10}$$

The Hamiltonian in equation 5.8 is a Hermitian operator, and the eigenvalues of a Hermitian operator must be real, so E is real. This means that the solutions f(t) are purely oscillatory since f(t) never changes in magnitude (recall Euler's formula $e^{\pm i\theta} = \cos\theta \pm i\sin\theta$) Thus, if:

$$\psi(r,t) = \psi(r)e^{-iEt/\hbar} \tag{5.11}$$

then the total wavefunction $\psi(r,t)$ differs from $\psi(r)$ only by a phase factor of a constant magnitude. There are some interesting consequences of this. Firstly, the quantity $\psi(r,t)^2$ is time-independent, as we can easily show:

$$\left|\psi(r,t)^2\right| = \psi^*(r,t)\psi(r,t) = e^{-iEt/\hbar}\psi^*(r)e^{-iEt/\hbar}\psi(r) = \psi^*(r)\psi(r) \tag{5.12}$$

5.4 PROPERTIES

The properties which are calculated to make inference to the research under study are discussed briefly below:

5.4.1 Geometry Optimization

Geometry optimization allows us to locate a minimum energy on the surface of potential energy, and thus achieve the equilibrium structure of a molecular system. So, what is sought is where the energy gradient that is equal to zero, but does not only occurs for the minimum, but also for the saddle points.

Optimization is complete when the forces are zero, and once completed, optimized parameters appear, expressed in link distances, link angles and dihedral angles[48].

5.4.2 Frequency

Frequency calculations are only valid at stationary points of the potential energy surface, so it is necessary that the calculation is carried out in an optimized geometry, for this reason, you should always run a geometry optimization before performing the calculation of frequencies[49]. The result of the frequency calculation allows to build the infrared spectrum of a molecular system.

5.4.3 Reactivity Indices

Within the framework of the theory of density functionalities, a formalism has been developed that allows to determine, from the parameters obtained from the calculation, properties such as ionization potential, electronic affinity, electronegativity, electrophilicity index, and chemical hardness, among others, which allow to establish the reactivity of the molecular systems.

In addition to the above, it can be mentioned that a reaction usually involves a change in electronic density and this can be quantified through the functions of Fukui that tells us,

from the energy point of view, the most stable way to distribute the load that is transferred in a chemical event. That is, if the molecule is going to receive charge, the Fukui function associated with the charge acceptance process tells us in which parts the load is going to receive, while if the molecule is going to give charge, the Fukui function associated with the donation process will tell us from which regions it will donate. Thus, Fukui's function related to the process of accepting charge that describes the sites susceptible to receiving a nucleophilic attack, while Fukui's function related to the process of donating charge describes sites susceptible to receiving an electrophilic attack.

5.4.3.1 Ionization Potential

The ionization potential (I) is defined as the energy needed to separate an electron from a molecular system. This is calculated with the energy difference between the cation and the neutral species[50].

$$I = E_{(+1)} - E_{(0)} \tag{5.13}$$

5.4.3.2 Electron Affinity

An important property of molecular systems that influences their chemical behavior is their ability to accept electrons and thereby form anions[50]. This property is called electronic affinity (EA).

In terms of energy, electronic affinity is defined as the difference in energy between the neutral and reduced species of a system in their respective optimized geometries and is calculated with the following expression:

$$EA = E_{(0)} - E_{(-1)} \tag{5.14}$$

5.4.3.3 Electronegativity

It is a measure of the force with which the nuclei of atoms attract the electrons of Valencia with greater intensity.

It is the arithmetic average of ionization energy (I) and electron affinity (EA)[51].

$$\chi = \frac{I + EA}{2} \tag{5.15}$$

5.4.3.4 Hardness

Chemical Hardness (η) is a global property of the system and measures the resistance imposed by it to the change in its electronic distribution.

Hardness is a descriptor of reactivity, it has been defined as the second partial derivative with respect to the number of electrons[50]. And the corresponding equation for obtaining hardness is:

$$\eta = \frac{I - EA}{2} \tag{5.16}$$

5.4.3.5 Softness

Chemical softness (s) is an inverse of Chemical hardness

$$s = \frac{1}{\eta} \tag{5.17}$$

5.4.3.6 Electrophilicity Index

Electrophilicity (ω) is a measure of energy stabilization of the system when it is saturated with electrons that come from the external environment. This property is expressed

by the square of the chemical potential divided by the double product of chemical hardness[51].

$$\omega = \frac{\mu^2}{2\eta} \tag{5.18}$$

5.4.4 Electron Injection Properties

Electron injection is the emission of electrons from one solid into another, this process has different properties that must be taken into account to have a good electron injection, the properties considered for electron injection in this research are discussed as follows,

The electron transfer from a dye to a semiconductor and the rate of the charge transfer process can be derived from Marcus theory[42, 52, 53] as,

$$k_{inject} = \left(\frac{\pi}{\hbar^2 \lambda k_B T} \right)^{0.5} \left| V_{RP} \right|^2 e^{\left[\frac{-(\Delta G_{inject} + \lambda)^2}{4 \lambda k_B T} \right]} \tag{5.19}$$

In Equation 5.19, k_{inject} is the rate constant (in S^{-1}) of the electron injection from dye to TiO_2, the higher the electron injection, the best SPCE factor and most efficient the DSSC. K_BT is the Boltzmann thermal energy, $\hbar \left(\frac{h}{2\pi} \right)$ which is related to the Planck constant, ΔG_{inject} is the free energy of injection, λ is the reorganization energy of the system.

The reorganization energy λ can be separated into the sum of two primary components:

1. the hole reorganization energy λ_h and

2. the electron reorganization energy λ_e

The total reorganization energy (λ) could enhance the J_{sc}, the lower the value of λ, faster the rate of charge-carrier transport and the total reorganization energy (λ) is calculated using the equation[54, 55]:

$$\lambda = \lambda_h + \lambda_e$$

$$\lambda_h = (E_o^+ - E_+^+) + (E_+^o - E_o^o)$$

$$\lambda_e = (E_o^- - E_-^-) + (E_-^o - E_o^o)$$

Where $E_o^+(E_o^-)$ is the energy of the cation (anion) calculated with the optimized structure of the neutral molecule. Similarly, $E_+^+(E_-^-)$ is the energy of the cation (anion) calculated with the optimized cation (anion) structure, $E_+^o(E_-^o)$ is the energy of the neutral molecule calculated at the cationic (anionic) state. Finally, E_o^o is the energy of the neutral molecule at the ground state. Considering equation 1 $|V_{RP}|$ is the coupling constant. High value $|V_{RP}|$ leads to higher injection time and high value $|V_{RP}|$ will give better result for the sensitizer, best SPCE factor and most efficient DSSC.[53, 56] The Hsu et al.[56] explained that $|V_{RP}|$ can be evaluated as

$$|V_{RP}| = \frac{\Delta E_{RP}}{2} \tag{5.20}$$

Furthermore, the energy difference can be formally expressed within Koopmans approximation as

$$\Delta E_{RP} = \left[E_{LUMO}^{dye} + 2E_{HOMO}^{dye} \right] - \left[E_{LUMO}^{dye} + E_{HOMO}^{dye} + E_{CB}^{TiO_2} \right] \quad (5.21)$$

Where $E_{CB}^{TiO_2}$ is the conduction band edge. Though it is often difficult to accurately determine $E_{CB}^{TiO_2}$, because it is highly sensitive to the conditions like pH of the solution, thus we used $E_{CB}^{TiO_2}$ = -4.0 eV, which is the experimental value corresponding to conditions where the semiconductor is in contact with aqueous redox electrolytes of fixed pH 7.0[57]. In a closed-shell system, the HOMO energy is related to the potential of first oxidation (i.e., $-E_{HOMO}^{dye} = E_{ox}^{dye}$) As a result, Equation 5.32 becomes

$$\Delta E_{RP} = -\left[E_{ox}^{dye} + E_{CB}^{TiO_2} \right] \quad (5.22)$$

Considering equation 5.21, there is still need to calculate the free energy change, therefore the free energy change (eV) for the electron injection can be expressed as[57]

$$\Delta G_{inject} = E_{ox}^{dye*} - E_{CB}^{TiO_2} \quad (5.23)$$

When the entropic component can be neglected in the calculation of the injection energetic balance, ΔE_{RP} corresponds to the injection-free energy change ΔG_{inject}.

Where E_{ox}^{dye*} is the oxidation potential of the dye in the excited state, and $E_{CB}^{TiO_2}$ is the reduction potential of the semiconductor conduction band. For this reaction path, the excited-state oxidation potential can be extracted from the redox potential of the ground state, E_{ox}^{dye}, which has been calculated and the vertical transition energy corresponding to the photoinduced Intramolecular Charge Transfer (ICT),

$$E_{ox}^{dye}* = E_{ox}^{dye} - \lambda_{\max}^{ICT} \quad (5.24)$$

Where $\lambda_{\max}^{ICT}$ is the energy of the ICT. Note that this relation is only valid if the entropy change during the light absorption process can be neglected.

Another important concept is Dye regeneration ΔG_{reg}, which is an essential factor that determines the rate of dye recombination. A negative value ΔG_{reg} implies a low dye recombination and a low dye recombination increases the rate of electron injection in the dye. The dye regeneration ΔG_{reg} can be calculated by using equation 5.25:

$$\Delta G_{reg} = E_{ox}^{dye} + E_{redox}^{Electrolyte} \tag{5.25}$$

Where $E_{redox}^{Electrolyte}$ is the electrolyte redox potential (− 4.85 eV)[58].

Moreover, the light-harvesting efficiency (LHE) of the dye has to be as high as possible to maximize the photocurrent response. Here, LHE is expressed as[59]:

$$LHE = 1 - 10^{-A} = 1 - 10^{-f} \tag{5.26}$$

Where A (f) is the absorption (oscillator strength) of the dye associated with the $\lambda_{\max}^{ICT}$

An additional important parameter is the open-circuit voltage (V_{oc}), the electron injection from the E_{LUMO} of the dye to the conduction band (E_{CB}) of the semiconductor surface arises from the relationship between the open-circuit voltage (V_{oc}) and the dye E_{LUMO}, V_{oc} (eV) can be calculated using[60]:

$$V_{oc} = E_{LUMO} - E_{CB} \tag{5.27}$$

Sang-Aroon *et al* proved that equation 5.19 provided a low injection rate for systems with enough relaxation time after electronic excitation[60]. It has been noted that Marcus

theory gives a good result at low potentials but at high potentials, the result is very low[60]. At high potential means that E_o is greater than the reorganizing energy λ, where E_o is the ground rotation-vibration state, note that $E_o - E_c = \Delta G_{inject} + \lambda$ [60]. So, the rate constant and k_{inject} are very low when using equation 5.19. According to Tian *et al*, electron injection is necessary to take place into the conduction band of semiconductor from the dye in the range of pico or femtoseconds[61]. Also, it has been noted that equation 5.19 calculations are attributed to

1. The large uncertainty concerning the conformational space of the systems;
2. The error related to the different key parameters combined with the high numerical sensitivity of the exponential function;
3. The dye molecules are probably overestimated by the DFT analysis[62];

Due to this justification, a more redefined formula was derived from Helmholtz potential function

$$k_{inject} = \left(\frac{\pi}{\hbar^2 k_B T} \right)^{0.5} |V_{RP}| \left[-\Delta G_{inject} - \left(E_c - E_F - \lambda \right) \right]^{0.5} \tag{5.28}$$

Where E_C - E_F is the difference between the energy of the conduction band and the energy of the Fermi level for TiO_2, and this difference is 1.6 eV[62]. Equation 10 delivers an almost linear dependence of rate constant on free energy of injection at high potential. By using equation 5.28, one calculates rate constant which is more realistic for an injection.

5.4.4.1 Rate constant

Rate constant is the electron transfer from a dye to a semiconductor and the rate of the charge transfer process.

5.4.4.2 Reorganization energy

Reorganization energy λ is the energy cost due to geometry modifications to go from a neutral to a charged oligomer and vice versa. It is one of the key characteristics that control charge mobility in organic electronics.

5.4.4.3 Free energy change

The free energy change for electron injection (ΔG_{inject}) determines the electron injection rate and therefore the photocurrent in DSSCs and it can be viewed as the electron injection driving force.

5.4.4.4 Coupling constant

The coupling constant between the reagent and the product potential curves is denoted by V_{RP}. A high value of V_{RP} gives a higher injection time.

5.4.4.5 Dye regeneration

The dye regeneration energy (ΔG_{reg}) is an essential factor that determines the rate of dye recombination: a negative value of ΔG_{reg} implies a low dye recombination, and a low dye recombination increases the rate of electron injection in the dye [44].

5.4.4.6 Light harvesting efficiency

Light-harvesting efficiency is the fraction of light intensity absorbed by the dye at a certain wavelength in the DSSC. The light-harvesting efficiency (LHE) of the dye has to be as high as possible to maximize the photocurrent response.

5.4.4.7 Open circuit voltage

The open-circuit voltage V_{OC} is the electron injection from the E_{LUMO} of the dye to the conduction band (E_{CB}) of TiO_2 (101) anatase phase semiconductor surface.

5.5 MOLECULES

Anthocyanidins, a group of flavonoids found in fruits, leaves, and flowers, are water-soluble plant pigments that usually carry vivid colors ranging from red to blue[63]. They also have long been considered to have health benefits and widely used as food colorants. Compared to ruthenium-based dyes, anthocyanidins are metal-free, non-toxic and widely available at very low expense[64]. They also have enough hydroxyl groups to bind TiO_2 nanocrystallites and have been shown to be able to inject electrons into the TiO_2 conduction band at an ultrafast rate when excited with visible light. Several researchers have investigated anthocyanin as photosensitizer[63, 64].

Betalains are a class of red and yellow indole-derived pigments found in plants of the Caryophyllales. Betalains also occur in some higher-order fungi[65]. They are most often noticeable in the petals of flowers but may color the fruits, leaves, stems, and roots of plants that contain them. They include pigments such as those found in beets. The name "betalain"

comes from the Latin name of the common beet (*Beta vulgaris*), from which betalains were first extracted[66]. The deep red color of beets, bougainvillea, amaranth, and many cacti results from the presence of betalain pigments. The particular shades of red to purple are distinctive and unlike that of anthocyanin pigments found in most plants.

There are two categories of betalains:[65]

1. Betacyanins include the reddish to violet betalain pigments. Among the betacyanins present in plants include betanin, isobetanin, probetanin, and neobetanin.
2. Betaxanthins are those betalain pigments which appear yellow to orange. Among the betaxanthins present in plants include vulgaxanthin, miraxanthin, portulaxanthin, and indicaxanthin.

VI. MATERIALS AND METHODS

6.1 EQUIPMENT

The equipment used for this work are Dell Precision T7400 Intel ® Xenon ® CPU 320GHz 2.66GHz, 4.00 GB RAM and the high-performance cluster with 8 nodes of 16 cores with 64GB in RAM named Prometeo.

6.2 PROGRAMS AND APPLICATIONS

The programs used are the suitable computational chemistry software Gaussian 09W[67], it graphic interface, Gauss View 5.0[68] to perform the studied molecular systems calculations. For the analysis of results the applications used are SpecDis[69], SWizard[70], Molview[71], ChemDoodle[72], Origin 10[73]

6.3 MOLECULES ANALYZED

The molecules systems included in this research are Aurantinidin, Cynadin, Delphinidin, Pelargonidin from anthocyanidin family (Figure 1). Betanidin, Isobetanidin, Indicaxanthin and Portulaxanthin from Betalain family (Figure 2). Also four modified molecules, tagged as follows: RAA, RBB, DAAA, DBAA, TACAA and TAPCAA. The Modified systems were carried out as shown in figures 3and 4. These modifications were done according to different methodologies describes below:

1. Two units of each dyes are connected by a vinyl group and Rhodanine-3-acetic acid added as the electron acceptor. For the Aurantinidin modified molecule, the IUPAC name is 2-(4-{2-[4-(7-{2-[(2,2-dihydroxyethyl)(disulfanylmethyl)amino]-2-hydroxy ethyl}-3,5,6-trihydroxy-octahydro-2H-1-benzopyran-2-yl)cyclohexyl]ethyl}cyclo

hexyl)-octahydro-2H-1-benzopyran-3,5,6,7-tetrol with a decided given name as Rhodanine-3-acetic acid-aurantinidin-aurantinidin, and for easy referencing, it was called RAA. While for Betanidin modified molecule, the IUPAC name is (4S,8S)-2-{2-[(2S)-5-[3-(2,2-dihydroxyethyl)-4-hydroxy-2-sulfanyl-1,3-thiazolidin-5-yl]-2-(dihydroxymethyl)-6-hydroxy-octahydro-1H-indol-1-yl]ethyl}-4,8-bis(dihydroxymethyl)-10-{2-[(2S)-2-(dihydroxymethyl)-5,6-dihydroxy-octahydro-1H-indol-1-yl]ethyl}-etradecahydro-13lambda3,14-dioxa-5,7-diazatetraphene-12,15-diol with a decided given name as Rhodanine-3-acetic acid-betanidin-betanidin, and for easy referencing, it was called RBB.

2. A design of the D-π-A structure of Aurantinidin and Betanidin will be introduced to broaden the dye's absorbance up to the near-infrared spectrum by the additions of diphenylamine as donor moiety and acrylic acid as acceptor moiety. For the Aurantinidin modified molecule, the IUPAC name is 7-(dicyclohexylamino)-2-[4-(3,3-dihydroxypropyl)cyclohexyl]-octahydro-2H-1-benzopyran-3,5,6-triol with a decided given name as diphenylamine-aurantinidin-acrylic acid, and for easy referencing, it was called DAAA. While for Betanidin modified molecule, the IUPAC name is 3-[(2S)-4-{2-[(2S)-5-(dicyclohexylamino)-2-(dihydroxymethyl)-6-hydroxy-octahydro-1H-indol-1-yl]ethyl}-2,6-bis(dihydroxymethyl)piperidin-1-yl]propane-1,1-diol with a decided given name as diphenylamine-betanidin-acrylic acid, and for easy referencing, it was called DBAA.

3. A design of D-π-A structure of Aurantinidin was done by the additions of triphenylamine as donor moiety and cyanoacrylic acid as acceptor moiety. For this Aurantindin modified molecule, the IUPAC name is 2-{4-[2-(aminomethyl)-3,3-

dihydroxypropoxy]cyclohexyl}-7-(tricyclohexylamino)-octahydro-2H-1-benzopyran-3,5,6-triol with a decided given name as triphenylamine-aurantinidin-cyanoacrylic acid, and for easy referencing, it was called TACAA.

4. A design of D-π-A structure of Aurantinidin was done by the additions of triphenylamine as donor moiety and phenyl-cyanoacrylic acid as acceptor moiety. For this Aurantindin modified molecule, the IUPAC name is 2-[4-({7-[2-(aminomethyl)-3,3-dihydroxypropyl]-octahydro-1H-inden-4-yl}methoxy)cyclohexyl]-7-(tricyclo hexylamino)-octahydro-2H-1-benzopyran-3,5,6-triol with a decided given name as triphenylamine-aurantinidin- phenyl-cyanoacrylic acid, and for easy referencing, it was called TAPCAA.

The photovoltaic properties of these four new modified molecules were calculated to identify the effect of the molecular arrangements on the DSSC performance.

More importantly, organic dyes must possess broad and intense spectral absorption in the visible light region and have good excited-state redox potential with the energy of the conduction band edge to be able to function well in a DSSC. The major factors that cause low conversion efficiency of DSSCs based on organic dyes are the formation of dye aggregation on the semiconductor surface and the recombination of conduction band electrons with triiodide in the electrolyte. Furthermore, two molecular arrangements were carried out on Aurantinidin because it shows better injection properties from the previous molecular arrangements.

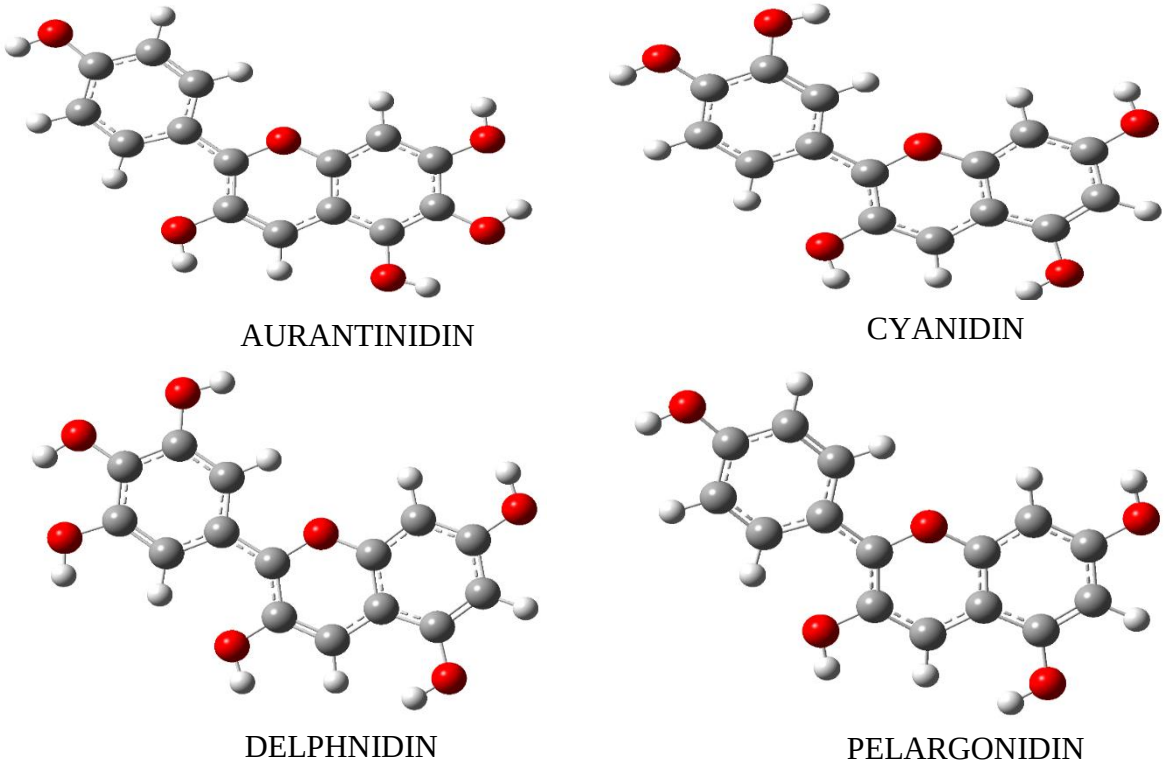

Figure 1. Schematic Structure of selected Anthocyanidin Family

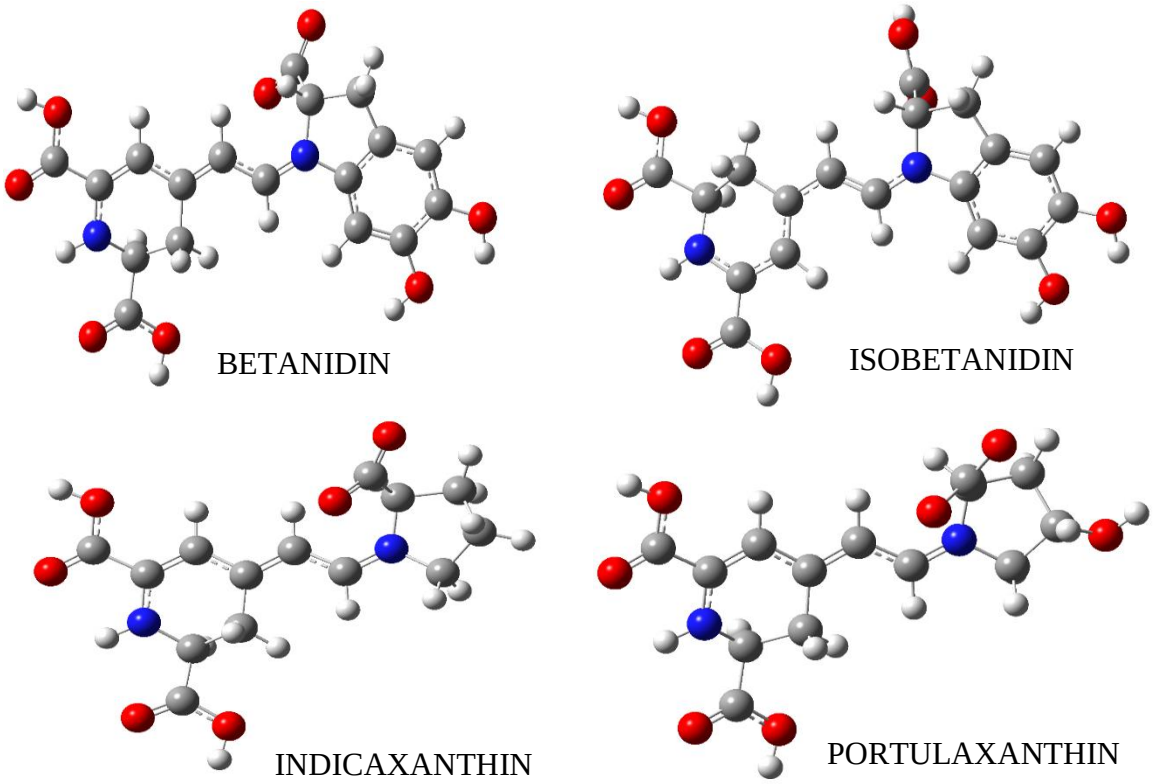

Figure 2. Schematic Structure of selected Betalain Family

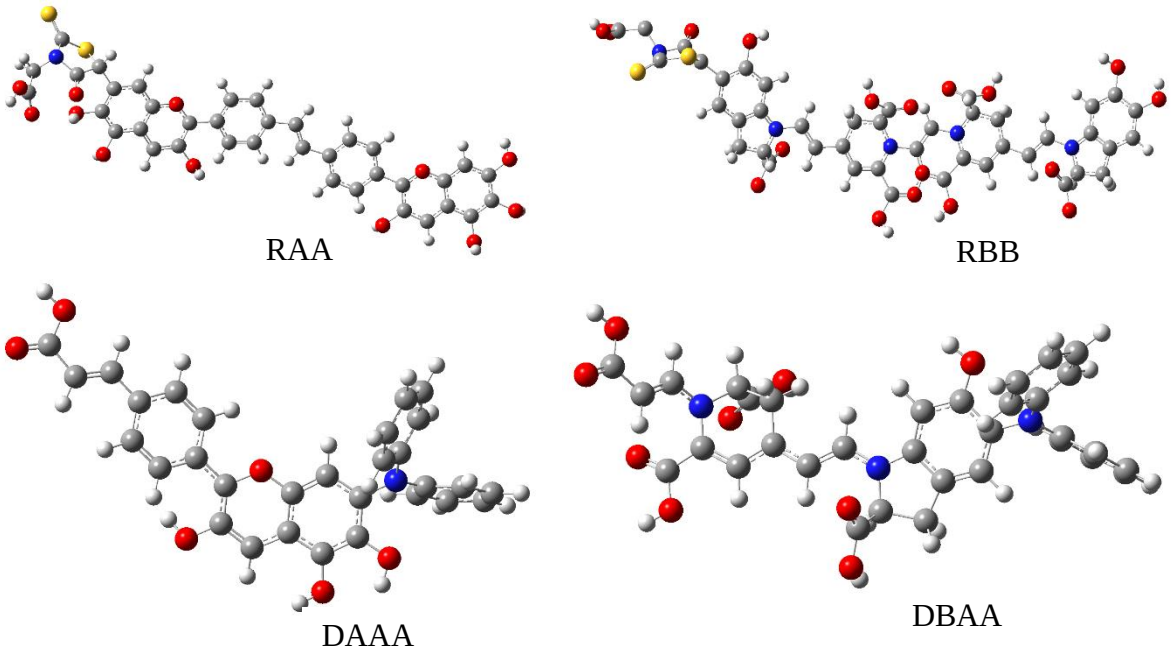

Figure 3. Schematic Structure of modification 1 done on Aurantinidin and Betanidin

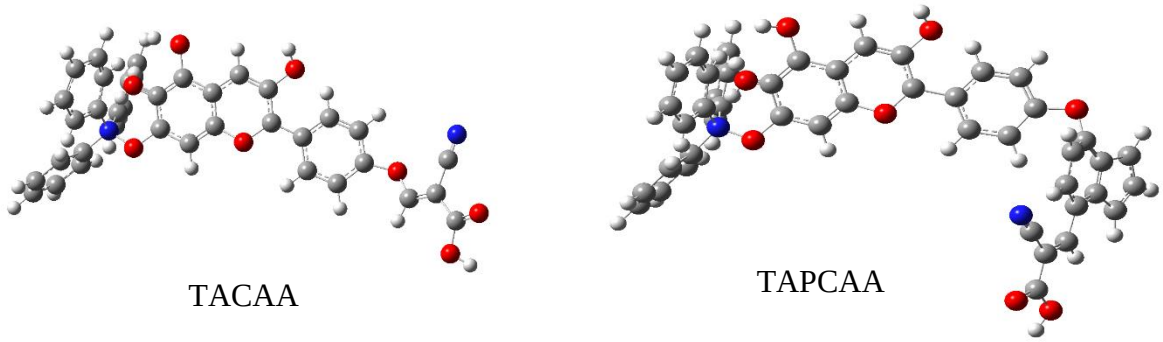

Figure 4. Schematic Structure of modification 2 done on Aurantinidin

6.4 COMPUTATIONAL DETAILS

The validation process was done using M06[74], M06L[75], B3LYP[76, 77] and MN12SX[78] functionals with 6-311+G(d,p)[79] basis sets to know the fuctional that gives more accurate results when compare to experimental results. The geometry optimizations of the structures were thereafter computed using Density Functional Theory (DFT) with the

Gaussian09 package[67]. The MN12SX functional and the 6-311+G(d,p) basis set were used for the analysis of the structures after found it as the better agreement with experimental properties as maximum wavelength (λ_{max}) and geometrical indices. The basis set has been chosen because it has been shown that return a converged λ_{max} for a series of calculations, while a smaller basis set would give a too short λ_{max} (in nm)[80].

The MN12SX functional belongs to the Minnesota family which is characterized by all parameterization against a broad range of chemical data. It belongs to the non-separable gradient approximation functionals that include exchange and correlation in the form of a non-separable gradient improvement of uniform electron gas exchange. Particularly, MN12SX was constructed adding both, kinetic energy density and screened exchange. The functional coefficients were optimized on a training of 369 chemistry and physics data, both chemistry energetic and structural data. The performance of the functional was probed on a set of databases, and results show that the functional provides broadly accurate performance for all chemistry and solid-state physics databases considered and has an excellent performance for chemistry and physics and for energies and structures[78].

VII. RESULTS AND DISCUSSION

7.1 VALIDATION

During a computational study or analysis, a best methodology to be used for computation must undergo a validation process, where different functionals and basis sets will be subjected for geometry and frequency calculation to determine the minimum energy and point, the most appropriate that is closer to experimental results of geometry indices and maximum wavelength will be considered. In this research, the validation was done using cyanidin and pelargonidin as case study with four different functionals and a basis set. This was generalized as an approximate validation for Anthocyanidin family, experimental values were gotten for the maximum wavelength and geometrical indices for the said molecules and were compared with our theoretical calculations.

7.1.1 Molecular Geometries

After the optimization of Cyanidin and Pelargonidin using the four functionals as shown in figure 7.1, the molecular structures were not twisted and they all stay plane. The presence of the hydroxyl in all the molecules helps in the non-twisting ability and thereby making the molecules to be plane. A non-twisted molecule produces a better overall conversion efficiency[81], which makes this family a good dye for a DSSC.

Cyanidin and Pelargonidin were characterized at four different functionals. The obtained results show a good agreement between the experimental and calculated bond length values of each of the functionals used in the computation. However, there is need to check the functional that gives the most accurate results. To make an extensive study of the

validation, a statistical technique known as population standard deviation was used on the results of the bond lengths. In this statistical technique, the experimental result was used as the reference, in this way, any functional that gives the lowest deviation will be the one that gives the most accurate result. Tables 7.1 and 7.2 show the experimental and calculated bond length of cyanidin and pelargonidin respectively. The results of the population standard deviation shows that MN12SX/6-311+G(d,p) gives the most accurate result because it has the lowest deviation.

Table 7.1. Experimental and Computational values of Bond Length of Cyanidin showing standard deviation using 6-311+G(d,p) basis set

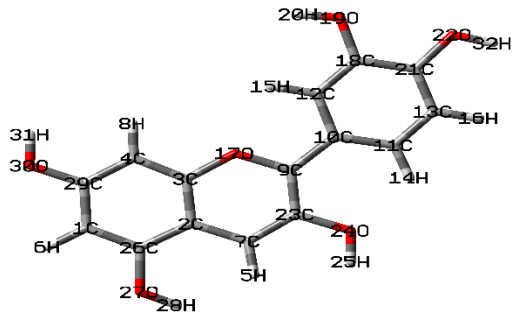

Bond length	Experimental	B3LYP	M06L	M06	MN12SX
9C– 17O	1.3490	1.3904	1.3877	1.3805	1.3801
9C – 23C	1.3960	1.3999	1.3988	1.3983	1.3963
7C – 23C	1.3800	1.3886	1.3865	1.3818	1.3824
2C – 7C	1.3820	1.4327	1.4265	1.4277	1.4278
2C – 26C	1.4320	1.4140	1.4115	1.4081	1.4072
1C – 26C	1.3660	1.3869	1.3856	1.3837	1.3817
1C – 29C	1.4130	1.3948	1.3924	1.3905	1.3894
4C – 29C	1.3870	1.3953	1.3936	1.3902	1.3902
3C – 4C	1.3760	1.3890	1.3864	1.3845	1.3843
3C – 17O	1.3610	1.3657	1.3605	1.3558	1.3553
2C – 3C	1.4080	1.4061	1.4044	1.4011	1.3997
9C – 10C	1.4530	1.4481	1.4387	1.4419	1.4415
10C – 12C	1.4090	1.4157	1.4140	1.4107	1.4095
12C – 18C	1.3710	1.3853	1.3824	1.3806	1.3797
18C – 21C	1.4000	1.4051	1.4038	1.4002	1.4004
13C – 21C	1.3780	1.3928	1.3906	1.3873	1.3867
11C – 13C	1.3830	1.3890	1.3862	1.3843	1.3836
10C – 11C	1.4040	1.4109	1.4099	1.4067	1.4045
	STD	**0.0192**	**0.0179**	**0.0170**	**0.0170**

Experimental[82]

Table 7.2. Experimental and Computational values of Bond Length of Pelargonidin showing standard deviation using 6-311+G(d,p) basis set

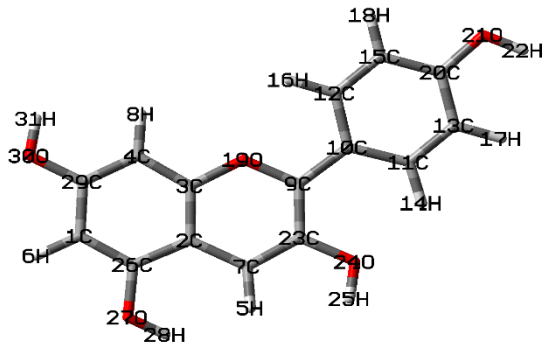

Bond length	Experimental	B3LYP	M06L	M06	MN12SX
9C– 19O	1.3790	1.3785	1.3872	1.3894	1.3904
9C – 23C	1.4320	1.3957	1.3989	1.3993	1.4016
7C – 23C	1.3940	1.3837	1.3862	1.3892	1.3883
2C – 7C	1.4160	1.4284	1.4255	1.4325	1.4326
2C – 26C	1.4330	1.4076	1.4112	1.414	1.4149
1C – 26C	1.3890	1.3818	1.3853	1.3868	1.389
1C – 29C	1.4220	1.3899	1.3924	1.395	1.3957
4C – 29C	1.4090	1.3896	1.3941	1.3952	1.3952
3C – 4C	1.3950	1.3835	1.3864	1.3889	1.3891
3C – 19O	1.3870	1.3543	1.3607	1.3652	1.366
2C – 3C	1.4210	1.4001	1.405	1.4064	1.4078
9C – 10C	1.4390	1.4434	1.4398	1.4496	1.4495
10C – 12C	1.4350	1.4101	1.4149	1.4163	1.4176
12C – 15C	1.3860	1.3787	1.3812	1.3848	1.3864
15C – 20C	1.4190	1.3902	1.3942	1.3954	1.3964
13C – 20C	1.4160	1.3906	1.3947	1.3961	1.397
11C – 13C	1.3930	1.3823	1.3837	1.3879	1.3886
10C – 11C	1.4310	1.4069	1.4118	1.4132	1.4151
	STD	**0.0219**	**0.0185**	**0.0175**	**0.0167**

Experimental[83]

7.1.2 Electronic Absorption Spectral

The absorption spectra found with the four different functional for Cyanidin and Pelargonidin were compared. Within the investigated visible absorption spectrum range of 400 – 600nm, they all show maxima peaks. The different functionals and basis set used for the validation of the methodology were found to have produced spectra in good order which agrees with experimental results. The computed UV-visible absorption data are shown in Tables 7.3

Table 7.3. Absorption wavelength (nm), Oscillator strength for Anthocyanindin

	B3LYP			M06			M06L			MN12SX			EXP
Dyes	**λ(nm)**	**f**	**Transition (%)**	**λ(nm)**	**f**	**Transition (%)**	**λ(nm)**	**f**	**Transition (%)**	**λ(nm)**	**f**	**Transition (%)**	**λ_{max}(nm)**
	540.4	0.0011	H - L (69)	545.2	0.1120	H - L +3(64)	580.2	0.0003	H - L (62)	545.7	0.1392	H - L (96)	
										479.7	0.0484	H - L (96)	
	467.5	0.1638	H - L (21)	471.5	0.0039	H - L (93)	497.0	0.1115	H - L (26)				546
			H - L +1(16)						H - L +1(20)	467.1	0.1162	H - L (88)	
Cyanidin													
	419.3	0.2082	H - L +1(72)	460.9	0.0025	H - L +3(20)	461.9	0.1146	H - L +1(67)				
						H - L +6(16)			H - L +2(10)				
	549.0	0.0055	H - L (74)	544.2	0.0011	H - L +3(69)	577.5	0.0025	H - L (73)	551.0	0.2320	H - L (94)	
										488.0	0.0456	H - L (99)	
	466.9	0.1037	H - L (18)	470.8	0.1638	H - L (95)	513.8	0.0149	H - L +1(67)				550
			H - L +1(16)					0.0953	H - L (11)				
										450.1	0.0643	H - L+1 (11)	
Pelargonidin			H - L +2(12)										
										435.6	0.0517	H - L +1(36)	
	440.3	0.0520	H - L +1(75)	459.6	0.2082	H - L +3(19)	484.4		H - L +1(26)				
			H - L +2(10)			H - L +8(10)			H - L +2(20)				

λ_{max} [84]

As it can be noted in Table 7.3, all the spectral are in the range of 400-600nm and contributed to the transition. In this region, the simulated spectral shows several peaks, all the molecules have highest oscillator strength transition in the HOMO-LUMO transition level for three of the functionals, except M06 which shows transition in the HOMO-LUMO+3 level for both molecules.

The absorption strength is mainly determined by oscillator strength of the molecule, the higher the oscillator strength the better the absorption rate of the dye molecule and the better the electron transfer and once we have a good electron transfer from the dye to the semiconductor, this affects the efficiency of the DSSC in a positive way. MN12SX/6-311+G(d,p) shows a higher oscillator strength compared to other level of theories used for the validation process and a closer value of maximum wavelength to the experimental value.

7.1.3 Reactivity parameters

After the validation where a more accurate result from the wavelength and bond length analysis are for MN12SX/6-311+G(d,p), it was defined as the suitable methodology to be used to study the electron injection process. Also, is desirable to check the reactivity parameters using MN12SX to be able to know the band gap (ΔE_{Homo}-E_{Lumo}) of the molecule and also to confirm the activeness of the molecule, if it will facilitate the electron injection.

The results show a very close range of values for the hardness and softness as shown in table 7.4, because Cyanidin and Pelargonidin has the same value of band energy. The results show that Cyanidin and Pelargonidin will be chemically reactive and this makes it a good natural dye for DSSC considering the values for hardness and ionization and electron affinity parameters.

The lower the chemical hardness, the tendency of generating excellent photoelectric conversion efficiency is increased[50]. And so, the dye would have a higher short-circuit current density.

The LUMO energy values for all dyes are located above the conduction band edge of TiO_2 (-4.0 eV), also the Highest Occupied Molecular Orbital (HOMO) energy was below the redox mediator of I^-/I^{3-} (-4.85 eV). The relative matching of electronic levels of sensitizers would lead to energetically favorable electron injection as well as regeneration of oxidized dye during DSSC operation. It was also noted that in both phases, the energy gap was very close even some molecules have the same value in both phases.

Table 7.4. Reactivity Parameters for Anthocyanidin

Dyes	E_{Lumo} (eV)	E_{Homo} (eV)	Energy Gap (eV)	I (eV)	A(eV)	χ (eV)	η (eV)	S (eV^{-1})	μ (eV)	ω (eV^{-1})
Cyanidin	-5.85	-2.45	3.40	4.19	2.72	3.45	1.47	0.68	-3.45	4.07
Pelargonidin	-5.73	-2.33	3.40	4.17	2.69	3.43	1.48	0.68	-3.43	3.99

7.2 RESULTS ON ANTHOCYANIDIN AND BETALAIN

MN12SX functional was decided as a better functional to be used for the detail computational analysis of this research, computational analysis of Anthocyanidin and betalain families were done to determine the electron injection.

7.2.1 Geometry Optimization

Aurantinidin, Cyanidin, Delphinidin and Pelargonodin were selected from the Anthocyanidin family and these dyes were selected because they have a similar orientation

of the radical atoms of either –H or –OH. Betalain families were carefully studied and from the two classes of Betalain, which are Betacyanin and Betaxanthins, two dyes were considered from each class. For the Betacyanin class, we considered the aglycone nature of this class, which are Betanidin and Isobetanidin and for Betaxanthins, we considered Indicaxanthin and Portulaxanthin. The optimized molecular structure of these dyes are shown at the molecules analyzed section (Section 6.3).

It was found that after the optimization of all the selected Anthocyanidin and betalain families, the molecular structures were not twisted and they all stay plane. As it was stated in the validation section, the presence of the hydroxyl in all the molecules helps in the non-twisting ability and thereby making the molecules to be flat. A non-overlap of atoms of a molecule produces a better overall conversion efficiency, which makes this family a good dye for a DSSC.

7.2.2 Optical Properties

The absorption spectra of the dye molecules were compared, the computed UV-visible absorption data of the dyes are shown in Tables 7.5 and 7.6. Within the investigated visible absorption spectrum range of 400 – 600nm, they all show maxima peaks.

All the dyes have highest oscillator strength transition in the HOMO-LUMO transition level. It was also noted that Betaxanthin (Indicaxanthin and Portulaxanthin) has relative lower wavelengths compared to all selected dyes. This can be attributed to the presence of one benzene ring in the betaxanthin family. Benzene ring has aromaticity with π-electron and these rings seem to be a factor that increases the wavelength of the molecule with more than one ring.

Table 7.5. Absorption wavelength (nm), Oscillator strength and transition levels for Anthocyanidin

MN12SX/6-311+G(d,p)			
Dyes	**λ(nm)**	**f**	**Transition (%)**
Aurantinidin	547.8	0.2453	H - L (73)
	487.7	0.0780	H - L (65)
			H - L +1(26)
	427.7	0.1209	H - L +1(27)
	414.6	0.0074	H - L +1(27)
	403.0	0.0011	H - L (42)
			H - L +1(18)
Cyanidin	545.7	0.1392	H - L (96)
	479.7	0.0484	H - L (96)
	467.1	0.1162	H - L (88)
	456.3	0.0326	H - L (74)
			H – L+1 (14)
	445.8	0.0367	H – L+1 (67)
	440.5	0.0391	H - L (64)
	407.4	0.0121	H – L+2 (40)
Delphinidin	569.8	0.1339	H - L (93)
	487.5	0.0871	H - L (99)
	460.9	0.0942	H - L +1(34)
	438.5	0.0146	H - L (67)
			H - L +1(14)
Pelargonidin	551.0	0.2320	H - L (94)
	488.0	0.0456	H - L (99)
	450.1	0.0643	H - L+1 (11)
	435.6	0.0517	H - L +1(36)

Table 7.6. Absorption wavelength (nm), Oscillator strength and transition levels for Betalain

MN12-SX/6-311+G(d,p)			
Dyes	**λ(nm)**	**f**	**Transition (%)**
Betanidin	549.4	0.1849	H - L (54)
	507.5	0.1809	H - L +2(48)
	462.4	0.6234	H - L +2(53)
	407.6	0.0009	H - L (74)
			H – L+1 (23)
Indicaxanthin	525.6	0.2287	H - L (71)
	504.3	0.0516	H – L+1 (47)
	484.1	0.1324	H – L+2 (53)
	438.3	0.0180	H - L (98)
Isobetanidin	536.3	0.2479	H - L (97)
	480.2	0.0523	H – L+2 (96)
	436.7	0.0169	H - L +1(67)
	408.0	0.0108	H - L (71)
			H - L +1(14)
Portulaxanthin	510.8	0.3104	H - L (77)
	492.0	0.1015	H – L+1 (63)
	475.2	0.0340	H - L+2 (80)
	427.7	0.0121	H - L +1(57)

7.2.3 Energy band Gap

The LUMO energy values for all the dyes are located above the conduction band edge of TiO_2 (-4.0 eV), also the Highest Occupied Molecular Orbital (HOMO) energy was below the redox mediator of I^-/I^{3-} (-4.85 eV) as shown in our results in table 7.7 and 7.8. The relative matching of electronic levels of sensitizers would lead to energetically favorable electron injection as well as regeneration of oxidized dye during DSSC operation. It was also noted that, the energy gap was very close even some molecules have the same value.

Table 7.7. Energy Levels for Anthocyanidin

Anthocyanidin	HOMO (eV)	LUMO (eV)	HOMO-LUMO Gap (eV)
Aurantinidin	-5.82	-2.56	3.26
Cyanidin	-5.85	-2.45	3.40
Delphinidin	-5.83	-2.52	3.31
Pelargonidin	-5.73	-2.33	3.40

Table 7.8. Energy levels for Betalain

Betanidin	HOMO (eV)	LUMO (eV)	HOMO-LUMO Gap (eV)
Betanidin	-7.14	-3.58	3.56
Isobetanidin	-7.24	-3.66	3.58
Indicaxanthin	-7.06	-3.54	3.52
Portulaxanthin	-6.95	-3.70	3.25

7.2.4 Frontier orbitals

The driving force for the electron injection from a dye to a semiconducting oxide is the energy-level difference between the dye´s LUMO level and the E_{CB} of the semiconducting oxides. However, explaining the electron-injection efficiency only with the

dye´s required energy levels is not enough, because the degree of electron injection is also strongly affected by the molecular orientation and spatial arrangement of dyes, such as aggregation, and electronic coupling with the electrode[85].

Organic dye´s intrinsic properties, such as shape, geometry, and conjugation length, should also be considered in the dye design to improve electron-injection efficiency. Our results in figures 5 and 6 in the HOMO state, shows that the electron density of the dye is mostly localized around the electron-donating group. However, in the LUMO state the electrons are localized near the electron-withdrawing acceptor side. This indicates that electron should move from donor to acceptor after the light absorption through excitation, and the structure is advantageous to direct intramolecular electron transfer from donor to acceptor.

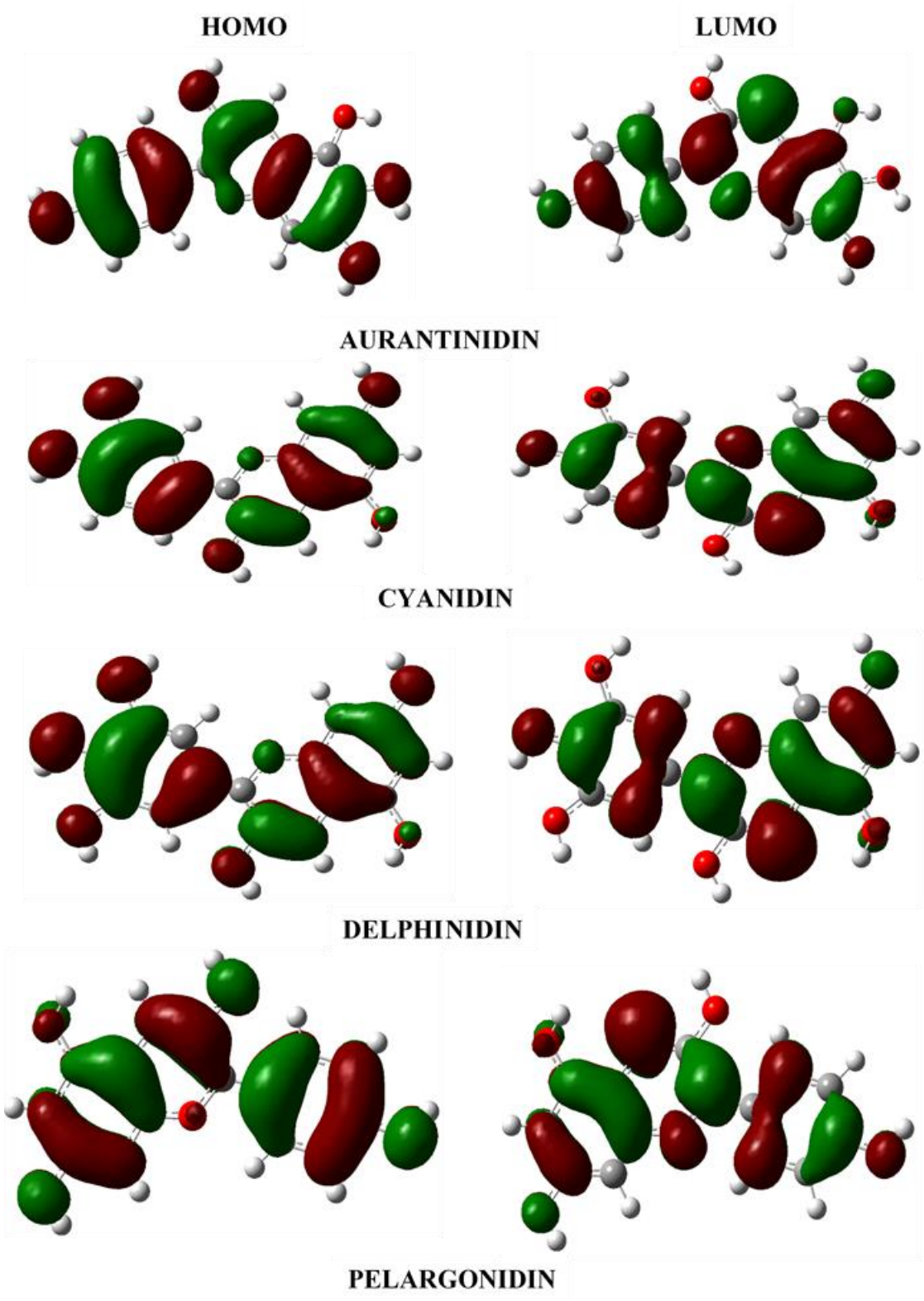

Figure 5. Molecular Orbital of selected Anthocyanidin family

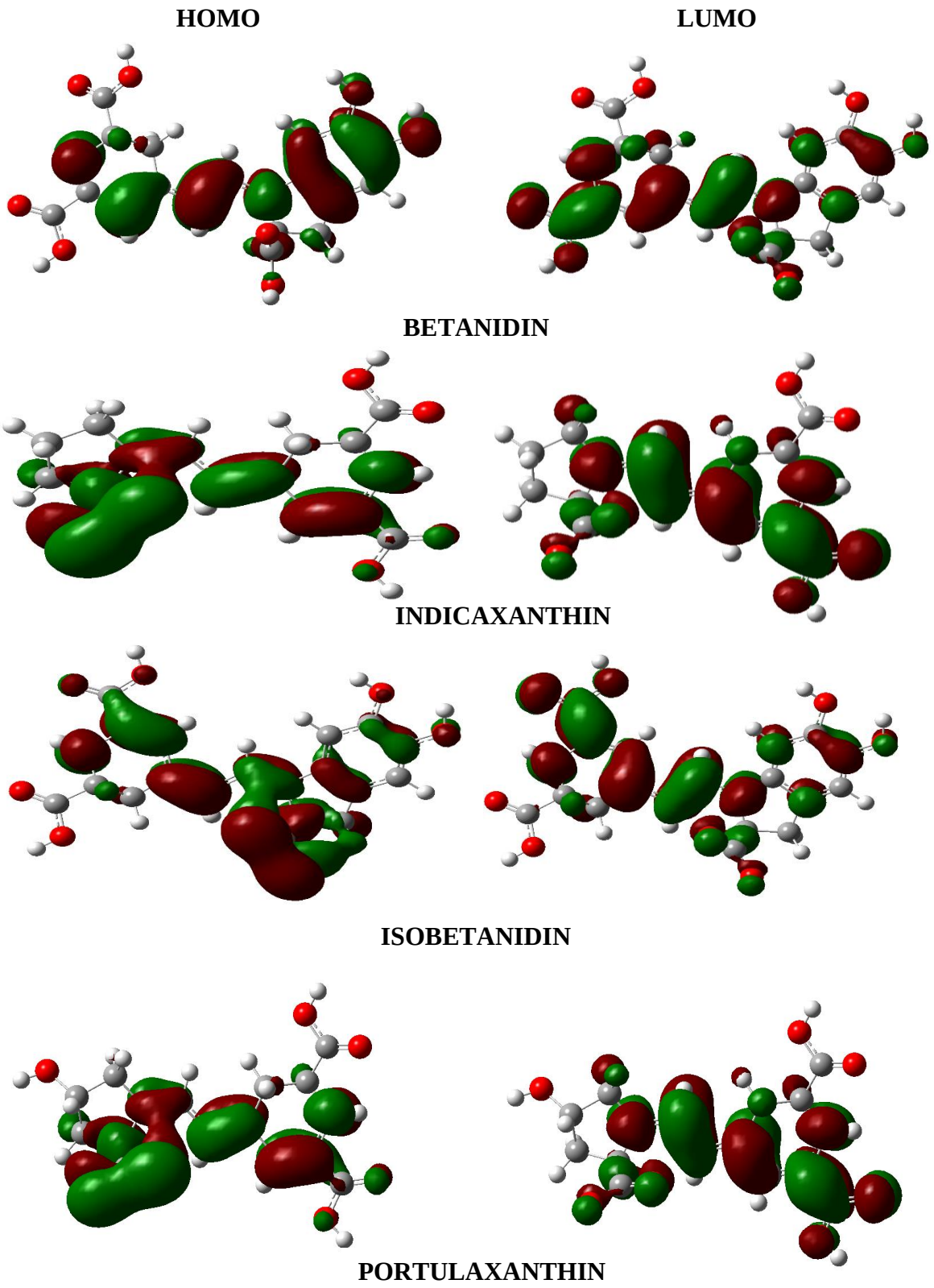

Figure 6. Molecular Orbital of selected Betalain family

7.2.5 Electron Injection

According to previous research, it has been demonstrated that the driving force - ΔG_{inject} of 0.20 eV was necessary for efficient dye regeneration[17]. It was observed that - ΔG_{inject} varies in values in the anthocyanidin family, ranging from 2.15 to 2.54. Also, the Betalain family has $-\Delta G_{inject}$ values ranging from 1.246 to 1.396. The value of $-\Delta G_{inject}$ for Anthocyanidin and Betalain families are above the required 0.2 eV for an electron injection to take place, this means that these values support good electron injection from the dye to the conduction band of the semiconductor materials.

It was observed that ΔG_{inject} are all negative and this indicate that all the selected dyes have excited states above the conduction band of the semicoinductor and this will make the dyes to easily inject electrons to the semiconductor materials.

It is also observed that ΔG_{reg} shows negative values for Anthocyanidin families, this indicates that the redox level of the electrolyte is lower than the ground states of the selected dyes. These particular attributes make the electron recombination to reduce. But for Betalain families, it shows a positive value for ΔG_{reg}, which will make electron recombination to be faster.

The rate constant k_{inject} of electron injection is very rapid from our results, which shows that the anthocyanidin and betalain families are good sensitizer for electron injection into the conduction band of the semiconductor material. Although, due to the value of ΔG_{reg} for Betalain families, electron recombination is higher. Aurantinidin has the highest rate constant of 2.64 X 10^{16} s^{-1} in the Anthocyanidin family. This indicates that among the anthocyanidin family, Aurantinidin gives a better electron injection value among the selected

dye having an injection time scale of 0.0379 fs because it has the highest electron injection value. Others also have a good value for rate constant. Betanidin has the highest rate constant of 9.84 X 10^{15} s^{-1} in the Betalain family giving a corresponding value of 0.1017 fs in the injection time scale.

Aurantinidin dye will give a good short-circuit current density J_{sc} because of its relative high LHE and k_{inject}, the higher the open-circuit voltage (V_{oc}) and the better the overall efficiency (η). V_{oc} values of this selected dye besides ΔG_{inject} and LHE is also another factor that affects efficiency. Anthocyanidin families give a better V_{oc} values. As the consequence of above organic dyes, we could predict that the Aurantinidin dye with large LHE, k_{inject} and a relatively high V_{oc} will have maximum efficiency. As it was described section 5.4.4.6, the light harvesting efficiency (LHE) is the efficiency of dye to response to light. It is another factor which indicates the efficiency of DSSC. The light harvesting efficiency (LHE) of the dye should be as high as feasible to maximize the photo-current response.

In this research, it was discovered that Anthocyanidin gives better injection ability than the Betalain family due to its high LHE, k_{inject} and V_{oc}, and this high value can be due to the numbers of benzene rings presence in Anthocyanidin family. Benzene ring gives more stability to a molecule due to the aromaticity nature. Injection time scale in fs (10^{-15}), k_{inject}, ΔG_{inject}, E_{ox}^{dye}, $E_{ox}^{dye}*$, λ_{max}^{ICT}, $|V_{RP}|$, ΔG_{reg}, f, LHE, V_{oc} for Anthocyanidin and Betalain families respectively are shown in tables 7.9 and 7.10.

Table 7.9. k_{inject}, ΔG_{inject}, $|V_{RP}|$, ΔG_{reg}, LHE and V_{oc} **for Anthocyanidin family**

Anthocyanidin	Injection Time Scale (fs)	k_{inject}	ΔG_{inject}	E_{ox}^{dye}	E_{ox}^{dye*}	$\lambda_{\max}^{ICT}$	$\lvert V_{RP}\rvert$	ΔG_{reg}	f	LHE	V_{oc}
Aurantinidin	0.0379	2.64 X 10^{16}	-2.54	3.72	1.46	2.26	0.715	-1.13	0.2453	0.4315	1.44
Cyanidin	0.0457	2.19 X 10^{16}	-2.29	3.98	1.71	2.27	0.765	-0.87	0.1392	0.2742	1.55
Delphinidin	0.0514	1.95 X 10^{16}	-2.15	4.03	1.85	2.18	0.800	-0.82	0.1339	0.2653	1.48
Pelargonidin	0.0453	2.21 X 10^{16}	-2.31	3.94	1.69	2.25	0.815	-0.91	0.2320	0.4139	1.67

Table 7.10. k_{inject}, ΔG_{inject}, $|V_{RP}|$, ΔG_{reg}, LHE and V_{oc} **for Betalain family**

Betanidin	Injection Time Scale (fs)	k_{inject}	ΔG_{inject}	E_{ox}^{dye}	E_{ox}^{dye*}	$\lambda_{\max}^{ICT}$	$\lvert V_{RP}\rvert$	ΔG_{reg}	F	LHE	V_{oc}
Betanidin	0.1017	9.84 X 10^{15}	-1.396	4.864	2.604	2.26	0.448	0.014	0.1849	0.3467	0.42
Isobetanidin	0.1289	7.76 X 10^{15}	-1.246	5.124	2.754	2.37	0.373	0.274	0.2479	0.4349	0.34
Indicaxanthin	0.1199	8.34 X 10^{15}	-1.300	5.060	2.700	2.36	0.400	0.210	0.2287	0.4094	0.46
Portulaxanthin	0.1045	9.57 X 10^{15}	-1.390	4.950	2.610	2.34	0.445	0.100	0.3104	0.5107	0.30

7.3 RESULTS ON THE MOLECULAR ARRANGEMENTS I

In this section we did two modifications on Aurantinidin and Betanidin, this two dyes were selected because they show good electron injection properties based on section 7.2. Two units of each dye are connected by a vinyl group and Rhodanine-3-acetic acid added as the electron acceptor. Aurantindin modified molecule will be labeled RAA while Betanidin modified molecule will be labeled RBB. A design of the D-π-A structure of Aurantinidin and Betanidin was done to broaden the dye's absorbance up to the near-infrared spectrum by the additions of diphenylamine as donor moiety and acrylic acid as acceptor moiety. Aurantindin modified molecule will be labeled DAAA while Betanidin modified molecule will be labeled DBAA.

7.3.1 Geometry Optimization

It was found that after the optimization that the molecular structures were not twisted and they all stay plane. As it was stated in the validation section, the presence of the hydroxyl in all the molecules helps in the non-twisting ability and thereby making the molecules to be flat. A non-overlap of atoms of a molecule produces a better overall conversion efficiency, which makes this family a good dye for a DSSC. The optimized molecular structure of RAA, RBB, DAAA and DBAA molecules are shown in Section 6.3.

7.3.2 Optical Properties

The absorption spectra of the modified molecules were compared. Within the investigated visible absorption spectrum range of 400 – 600nm, they all show maxima peaks. The computed UV-visible absorption data of RAA, RBB, DAAA and DBAA molecules are shown in Tables 7.11.

Table 7.11. Absorption wavelength (nm), Oscillator strength and transition level for modified molecules

Dyes	**MN12-SX/6-311+G(d,p)**		
	***λ*(nm)**	**f**	**Transition (%)**
RAA	744.5	0.3702	H - L (74)
	652.1	0.0087	H - L (11)
	645.4	0.1012	H - L (76)
	580.4	0.0004	H - L (99)
RBB	749.6	0.2162	H - L (79)
	731.1	0.0149	H – L+1 (19)
	618.1	0.0008	H - L +1(27)
	597.9	0.0153	H - L +1(71)
DAAA	569.8	0.1339	H - L (93)
	487.5	0.0871	H - L (99)
	460.9	0.0942	H - L +1(34)
	438.5	0.0146	H - L (67)
			H - L +1(14)
DBAA	551.0	0.2320	H - L (94)
	488.0	0.0456	H - L (99)
	450.1	0.0643	H - L+1 (11)
	435.6	0.0517	H - L +1(36)

7.3.3 Energy band Gap

The LUMO energy values for all dyes are located above the conduction band edge of TiO_2 (-4.0 eV), also the Highest Occupied Molecular Orbital (HOMO) energy was below the redox mediator of I^-/I^{3-} (-4.85 eV). The relative matching of electronic levels of sensitizers would lead to energetically favorable electron injection as well as regeneration of oxidized dye during DSSC operation. It was also noted that, the energy gap was very close even some molecules have the same value. Table 7.12 shows the HOMO, LUMO and energy band gap for RAA, RBB, DAAA and DBAA molecules.

Table 7.12. Energy Levels for Modified Molecules

Modified Molecules	HOMO (eV)	LUMO (eV)	HOMO-LUMO Gap (eV)
RAA	-5.54	-2.52	3.02
RBB	-4.94	-3.46	1.48
DAAA	-5.41	-2.68	2.73
DBAA	-5.31	-2.76	2.55

7.3.4 Frontier orbitals

HOMO orbital of the dyes are concentrated over donor unit, while the LUMO orbital are focused on the acceptor unit. This charge separation of HOMO and LUMO for dyes is benefit to electron injection from the excited dye to the conduction band of the semiconductor. It is clear that the modification of the structure has a significant effect on the molecular orbital of the dyes. Therefore, it was expected that the dyes will show a more effective intramolecular charge transfer (ICT) upon photoexcitation.

The electron distributions of the HOMOs and LUMOs of these dyes shows that HOMOs of the DAAA and DBAA dyes are distributed mainly over the entire diphenylamine

donor part, while the LUMOs are mainly delocalized over the π spacer and acrylic acid, while in RAA, the HOMO are localized around the Rhodanine-3-acetic acid, this arrangement might be due to the orientation of the –OH groups, the investigation of effect of functional group and position of functional group of dye on DSSC can serve as an important tool to guide further selection and synthesis of potential candidates as sensitizers [86]on Aurantinidin dyes when the two units are joined by a vinyl group, the LUMO of RAA are localized around the two units of the aurantinidin dye. RBB shows a different configuration when compared to RAA because it has HOMO that are localized around the two units of betanidin and the vinyl group, this orientation might be due to the presence of N-H path in the molecules, previous investigation into the position of functional groups has established this [86]. The insufficient overlap of the HOMO and LUMO orbitals in RAA and RBB implies that the strong acceptor may retard a fast charge transition from the donor to the anchor group, which is partly ascribed to the relatively low LHE compared to D-π-A formats. In order to identify the electron distribution and further understand the relationship between the electronic structure and electron transition, the frontier molecular orbitals diagram (HOMO and LUMO) of the dyes were obtained and are shown in Figure 7.

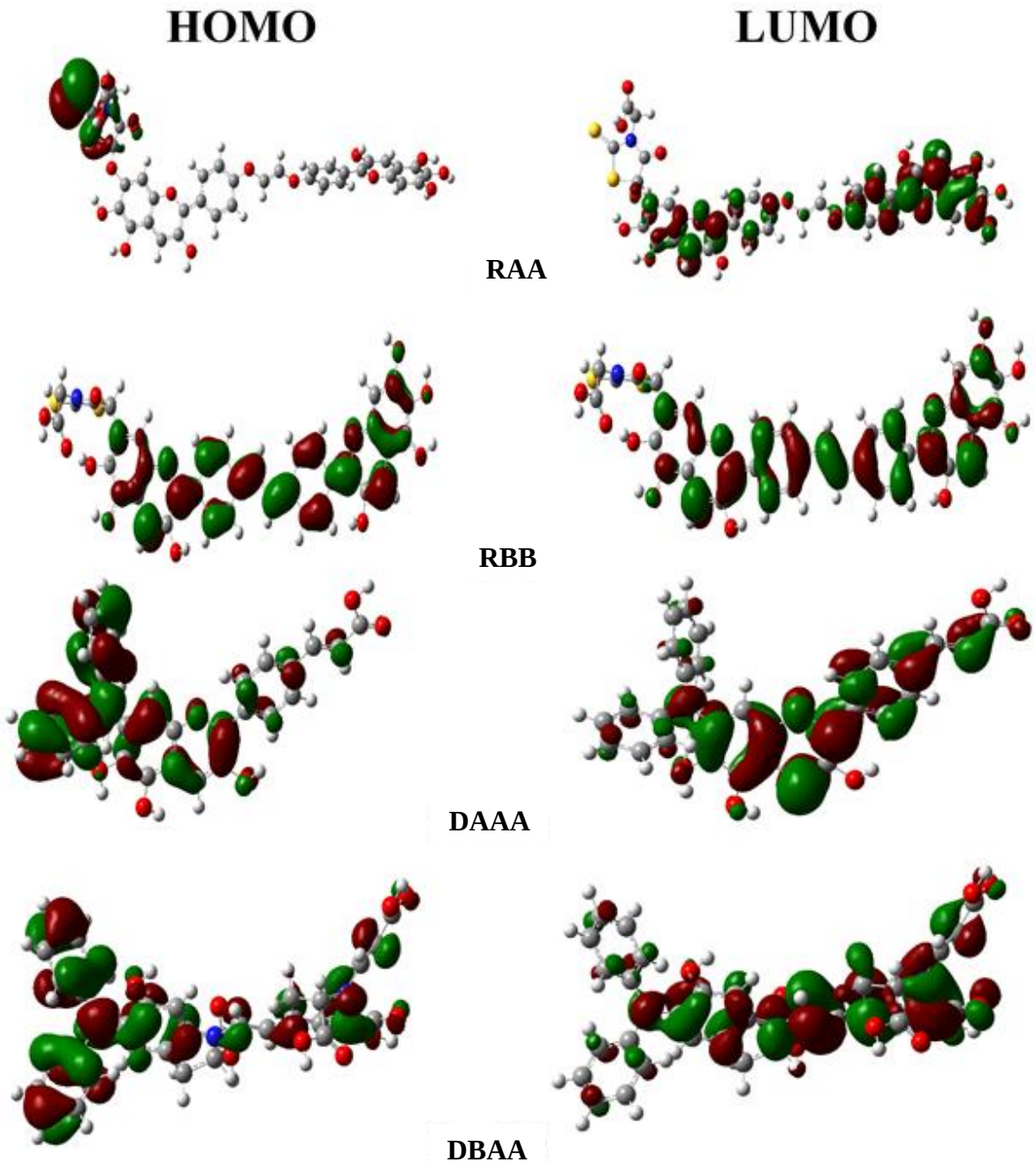

Figure 7. Molecular Orbital of Molecular Arrangements I

7.3.5 Electron Injection

It was observed that $-\Delta G_{inject}$ varies in values for the modified molecules, ranging from 1.33 to 2.9. The value of $-\Delta G_{inject}$ for the modified molecules are above the required 0.2 eV for an electron injection to take place, this means that these values support good electron injection from the dye to the conduction band of the semiconductor materials.

It was observed that ΔG_{inject} are all negative and this indicate that all the modified dye molecules have excited states above the conduction band of semiconductor and this will make the dyes to easily inject electrons to the semiconductor materials.

It is also observed that ΔG_{reg} shows negative values, this indicates that the redox level of the electrolyte is lower than the ground states of the selected dyes. These particular attributes make the electron recombination to reduce.

The rate constant k_{inject} of electron injection is very rapid, which shows that the modified molecules are good sensitizer for electron injection into the conduction band of the semiconductor material. DAAA has the highest rate constant of $3.26 \times 10^{16}\ s^{-1}$. This indicates that among the modified molecules, DAAA gives a better electron injection value among the selected dye having an injection time scale of 0.0307 fs because it has the highest electron injection value.

DAAA dye will give a good short-circuit current density J_{sc} because of its relative high LHE and k_{inject}, the higher the open-circuit voltage (V_{oc}) and the better the overall efficiency (η). V_{oc} values of this selected dye besides ΔG_{inject} and LHE is also another factor that affects efficiency. As the consequence of above organic dyes, we could predict that the DAAA dye with large LHE, k_{inject} and a relatively high V_{oc} will have maximum efficiency. The light harvesting efficiency (LHE) is the efficiency of dye to response to light. It is another

factor which indicates the efficiency of DSSC. The light harvesting efficiency (LHE) of the dye should be as high as feasible to maximize the photo-current response. The π bond is also another factor that gives this good results for DAAA.

To better predict the short-circuit photocurrent (J_{SC}) of dyes, light harvesting efficiency (LHE) and the driving force of electron injection (ΔG_{inject}) are calculated.

According to Equation (5.26), it is clear that light harvesting efficiency (LHE) is related to the oscillator strength (f). In order to obtain larger light harvesting efficiency (LHE), the oscillator strength (f) should be as higher as possible[87].

The results show that the modification of the dyes promote light harvesting efficiency (LHE) since the values increased when compared to previous work in section 7.2. Hence the dyes can absorb more photons, which is beneficial for improving short-circuit photocurrent (J_{SC})[88]. Another factor that influences short-circuit photocurrent (J_{SC}) is driving force of electron injection (ΔG_{inject})[88]. The values of ΔG_{inject} were negative, indicating that excited state dye lies above the conduction band (CB) of the semiconductor, and thus promote electron injection from the excited sensitizer to the semiconductor conduction band.

The dyes exhibit more negative driving force of electron injection (ΔG_{inject}), suggesting that they will exhibit faster electron injection. Also, the values found for force of electron injection indicates that the dyes will exhibit larger short-circuit photocurrent (J_{SC}). The reorganization energy (ΔG_{reg}) is another important factor that affects the short-circuit photocurrent (J_{SC}) of the DSSCs. Lower reorganization energy (ΔG_{reg}) will lead to faster electron transfer[89].

RBB has higher reorganization energy (ΔG_{reg}) value, because it has HOMO that are localized around the two units of betanidin and the vinyl group, this orientation might be due to the presence of N-H path in the molecules. Hence, the dyes will have higher power conversion efficiency due to the lower reorganization energy (ΔG_{reg})[90].

In this research, it was discovered that DAAA gives better injection ability among the modified dyes due to its high LHE, k_{inject} and V_{oc}, and this high value can be due to the numbers of benzene rings presence in Anthocyanidin family. Benzene ring gives more stability to a molecule due to the aromaticity nature.

In order to obtain larger V_{OC}, E_{LUMO} should be as higher as possible [91, 92]. The V_{OC} values of dyes are high. The modifications of the parent dyes not only increases short-circuit photocurrent (J_{SC}), but also enhances open-circuit photovoltage (V_{OC}). Table 7.13 shows electron injection properties for RAA, RBB, DAAA and DBAA systems.

Table 7.13. k_{inject}, ΔG_{inject}, $|V_{RP}|$, ΔG_{reg}, LHE and V_{oc} for Modified Molecules

Modified Molecules	**Injection Time Scale (fs)**	k_{inject}	ΔG_{inject}	E_{ox}^{dye}	$E_{ox}^{dye}*$	λ_{max}^{ICT}	$\lvert V_{RP}\rvert$	ΔG_{reg}	f	**LHE**	**V_{oc}**
RAA	0.0343	2.91 X 10^{16}	-1.33	4.34	2.67	1.67	0.665	-0.51	0.3702	0.5736	1.48
RBB	0.1053	9.57 X 10^{15}	-2.61	3.74	1.13	1.65	1.305	-1.11	0.2162	0.3921	0.54
DAAA	0.0307	3.26 X 10^{16}	-2.90	4.21	1.85	1.62	1.450	-0.64	0.3339	0.5419	1.32
DBAA	0.0362	2.77 X 10^{16}	-2.5	4.11	1.69	1.61	1.250	-0.74	0.2320	0.4139	1.24

7.4 RESULTS ON THE MOLECULAR ARRANGEMENTS II

A design of D-π-A structure of Aurantinidin was done by the additions of triphenylamine as donor moiety while cyanoacrylic acid and phenyl-cyanoacrylic were used separately as acceptor moiety.

7.4.1 Geometry Optimization

It was found that after the optimization that the molecular structures were not twisted and they all stay plane. A non-overlap of atoms of a molecule produces a better overall conversion efficiency, which makes this family a good dye for a DSSC. The optimized molecular structure of TACAA and TAPCAA molecules were shown in figure 4.

7.4.2 Optical Properties

Over the years, time-dependent DFT (TD-DFT) has been widely used in simulation of absorption and emission spectra. Therefore, absorption spectra of dyes were calculated based on the geometry optimization of the ground state.

The calculated oscillator strengths (f), absorption wavelengths, and electron transition are presented in Table 7.14. The maximum absorption peaks (λmax) of the dyes are found at 534.5–553.6 nm, which are all in visible region. It is the important region for photo-to-current conversion.

Absorption spectra shows that the dye exhibit a broad absorption band in the visible region, which is beneficial for improving the efficiency.

Table 7.14. Absorption wavelength (nm), Oscillator strength and transition level for modified molecules

	MN12-SX/6-311+G(d,p)		
Dyes	**λ(nm)**	**f**	**Transition (%)**
TACAA	553.6	0.3866	H - L (88)
	501.3	0.0259	H – L+1 (15)
	478.1	0.0048	H - L +1(32)
	457.6	0.0573	H - L +1(76)
TAPCAA	534.5	0.4066	H - L (82)
	502.3	0.0297	H - L (22)
	435.6	0.1054	H - L (72)
	400.4	0.0054	H - L (84)

7.4.3 Energy band Gap

The LUMO levels of dyes are in the range of -2.54 to -2.55 eV. Those values lie above the conduction band (CB) of the TiO_2 (-4.0 eV), indicating that excited state of the dyes could quickly and efficiently inject electrons into the TiO_2 conduction band. The HOMO levels of dyes are in the range of -4.86 to -4.87 eV. Those values are below the redox potential value of I^-/I^{-3} electrolyte (-4.85 eV), indicating that the oxidized dyes could quickly get electrons from the electrolyte. The molecular orbital energy of HOMO-LUMO configuration are computed as shown in table 7.15.

Table 7.15. Energy Levels for Modified Molecules

Dyes	HOMO (eV)	LUMO (eV)	HOMO-LUMO Gap (eV)
TACAA	-4.86	-2.55	2.31
TAPCAA	-4.87	-2.54	2.23

7.4.4 Frontier orbitals

The HOMO orbital of the dyes are concentrated over donor unit, while the LUMO orbital are focused on the acceptor unit. This charge separation of HOMO and LUMO for dyes is benefit to electron injection from the excited dye to the conduction band of the semiconductor. It is clear that the modification of the structure has a significant effect on the molecular orbital of the dyes. Therefore, the dyes will have more effective intramolecular charge transfer (ICT) upon photoexcitation.

The frontier molecular orbitals diagram (HOMO and LUMO) of the dyes are shown in Figure 8.

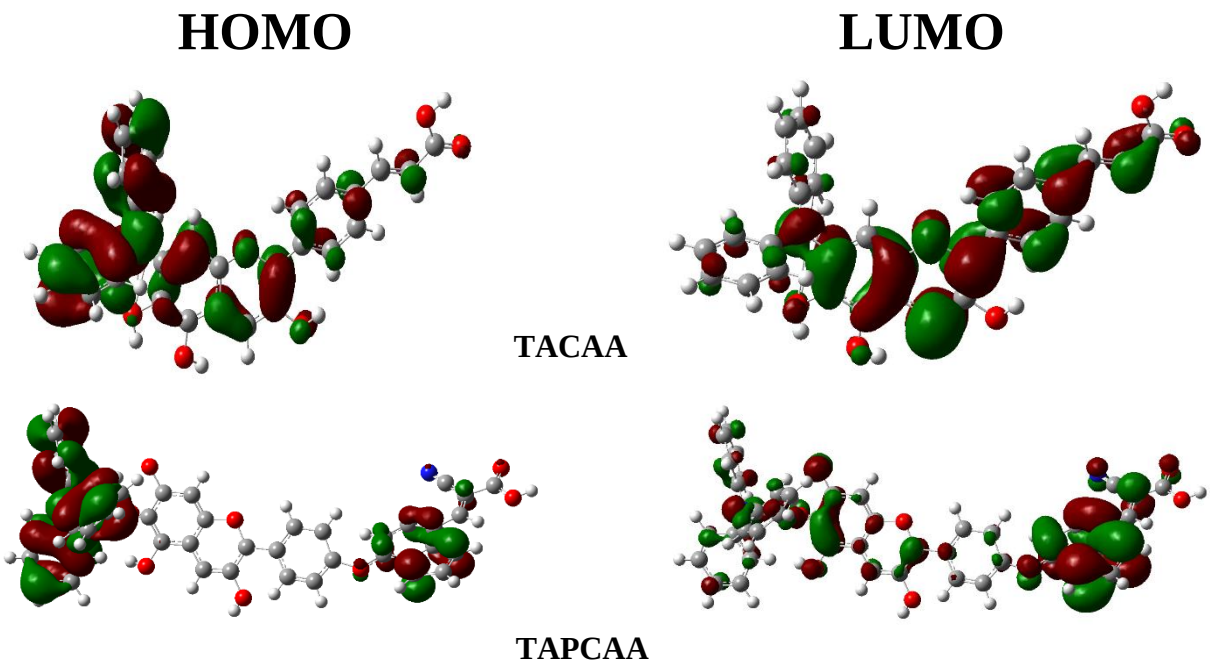

Figure 8. Molecular Orbital of Molecular Arrangements II

7.4.5 Electron Injection

To better predict the short-circuit photocurrent (J_{SC}) of dyes, light harvesting efficiency (LHE) and the driving force of electron injection (ΔG_{inject}) are calculated.

The results show that the modification of the dyes promote light harvesting efficiency (LHE) increase when compared to results from section 7.2 and 7.3. Hence the dyes can absorb more photons, which is beneficial for improving short-circuit photocurrent (J_{SC}). Another factor that influences short-circuit photocurrent (J_{SC}) is driving force of electron injection (ΔG_{inject}). Our results in Table 7.16 show, the values of ΔG_{inject} were negative, indicating that excited state dye lies above the conduction band (CB) of the TiO_2, and thus promote electron injection from the excited sensitizer to the TiO_2 conduction band.

The dyes exhibit more negative driving force of electron injection (ΔG_{inject}), suggesting that they will exhibit faster electron injection. At the same time, the ΔG_{inject} of dyes are larger than that of the non-modified studied systems. Therefore, dyes will exhibit larger short-circuit photocurrent (J_{SC}).

As shown in Table 7.16, the V_{OC} values of dyes are high. The modifications of the parent dyes not only increases short-circuit photocurrent (J_{SC}), but also enhances open-circuit photovoltage (V_{OC}).

Table 7.16. Calculated electronic properties of the dyes

Dyes	**LHE**	**ΔG_{inject}**	E_{ox}^{dye*}	E_{ox}^{dye}	**ΔG_{reg}**	**Voc**
TACAA	0.5894	-2.22	1.78	4.02	-0.83	1.45
TAPCAA	0.6079	-2.30	1.70	4.07	-0.78	1.46

VIII. CONCLUSIONS

In this research, the absorption spectral for the Cyanidin and Pelargonidin was studied using four functionals with 6-311+G(d.p) basis set for the validation process. The calculated geometric data indicate strong conjugation effects in these dyes, which are beneficial for the optical properties. UV-visible spectra were studied by TD-DFT for 20 excited states for each molecules and all shows peaks in UV visible region of 400-600nm.

It was observed that using MN12SX gives a closer value to the experimental value for the wavelength. The LUMO energy values for all dyes are located above the conduction band edge of TiO_2 (-4.0 eV) of the conduction band of TiO_2 nanoparticles and the Highest Occupied Molecular Orbital (HOMO) energy was below the redox mediator of I^-/I^{3-} (-4.85 eV), indicating possible electron injection from the LUMO of the dyes to the conduction band of the TiO_2 in DSSCs. Hence, MN12SX was the selected functional for this research.

According with the reactivity parameters calculated, anthocyanidin dye will be chemically reactive and this makes it a good natural dye for DSSC particularly, due to the values for hardness, ionization and electron affinity values.

The electronic structure of the selected Anthocyanidin and Betanidin was used to calculate the Optical properties and Energy band gap. The key parameters controlling the intramolecular charge transfer (ICT) injection and ET transfer rate constants were calculated.

The research shows that the rate constant of electron injection is very rapid, which shows that the selected families are good sensitizers for electron injection into the conduction band of the semiconductor material. Anthocyanidin family shows better injection ability

compared to the Betalain family due to the double aromatic ring they possess. The ΔG_{reg} factor constitute to the low electron injection of Betalain family because of the recombination nature of ΔG_{reg} value of the Betalain family. The light harvesting efficiency is large enough to maximize the photocurrent response.

The research shows that Aurantinidin dye is the best photosensitizer for DSSC from the selected dyes from both families been studied because it has good LHE, ΔG_{inject}, and relative high V_{oc}, Betanidin also shows a better result among the betalain family.

The research shows that the rate constant of electron injection is very rapid, which shows that the modified molecules are good sensitizers for electron injection into the conduction band of the semiconductor material. DAAA shows better injection ability due to the double aromatic ring they possess. The ΔG_{reg} factor constitute to the low electron injection of Betalain family because of the recombination nature of ΔG_{reg} value of the Betalain family. The light harvesting efficiency is large enough to maximize the photocurrent response.

DAAA dye is the best photosensitizer for DSSC from the modified molecules been studied because it has good LHE, ΔG_{inject}, and relative high V_{oc}.

TAPCAA shows better injection ability due to the double aromatic ring they possess. The light harvesting efficiency is large enough to maximize the photocurrent response.

TAPCAA dye is the best photosensitizer for DSSC from the modified molecules been studied because it has a relatively high value of LHE, ΔG_{inject}, and relative high V_{oc}.

IX. PUBLICATIONS AND CONFERENCES

Publications

Obasuyi, A.R., Glossman-Mitnik, D., Flores-Holguín, N.: Electron injection in anthocyanidin and betalain dyes for dye-sensitized solar cells: a DFT approach. J. Comput. Electron. 18, 396–406 (2019). https://doi.org/10.1007/s10825-019-01331-5

Obasuyi, A.R., Glossman-Mitnik, D., Flores-Holguín, N.: Theoretical Modifications of the molecular structure of Aurantinidin and Betanidin dyes to improve their efficiency as Dye Sensitized Solar Cells. J. Comput. Electron. (Under Review)

NOTE: copy of the published paper is attached under appendix

Conferences

Obasuyi Aanuoluwapo Raphael, Norma Flores-Holguín. DFT studies of maximum wavelength and geometric parameters of anthocyanidin using different methodologies. XVI Reunión Mexicana de FísicoQuímica Teórica. Puebla, México (16th – 18th November 2017) (Poster Presentation)

Obasuyi Aanuoluwapo Raphael, Daniel Glossman-Mitnik, Norma Flores-Holguín. Electron injection in anthocyanidin and betalain dyes for dye-sensitized solar cells: a DFT approach. XVII Reunión Mexicana de FísicoQuímica Teórica. Monterrey, México (22nd – 24th November 2018). (Oral Presentation)

Obasuyi Aanuoluwapo Raphael, Daniel Glossman-Mitnik, Norma Flores-Holguín. Modifications of the molecular structure of Aurantinidin for DSSCs. XVIII Reunión Mexicana de FísicoQuímica Teórica. Toluca, México (24th – 26th October 2019). (Poster Presentation)

Obasuyi Aanuoluwapo Raphael, Daniel Glossman-Mitnik, Norma Flores-Holguín. Sesión de posters de las Jornadas Académicas del Centro de Investigación en Materiales Avanzados (CIMAV), 25th Aniversario de CIMAV. Chihuahua, México (4th – 7th November 2019).

Scientific dissemination

Obasuyi Aanuoluwapo Raphael, Feria Infantil de Arte y Ciencia 2017. Held from April 25 to 30 por el Instituto Chihuahuense de la Cultura. Chihuahua, Chih

X. PERSPECTIVES AND RECOMMENDATIONS

It is recommended to corroborate the data obtained in this work through experimental techniques. It is suggested that more units of the dye molecules can be connected together and used as π as a further research when working with D-π-A molecular structures. For further research, more consideration can be placed on other donor and acceptor moieties apart from the ones used in this research.

XI. REFERENCES

1. Alsema, E.A.: Energy pay-back time and CO2 emissions of PV systems. Prog. Photovoltaics Res. Appl. 8, 17–25 (2000). https://doi.org/10.1002/(SICI)1099-159X(200001/02)8:1<17::AID-PIP295>3.0.CO;2-C

2. Kammen, D.M., Pacca, S.: Assessing the Costs of Electricity. Annu. Rev. Environ. Resour. 29, 301–344 (2004). https://doi.org/10.1146/annurev.energy.28.050302.105630

3. Service, R.F.: Is it time to shoot for the sun? Science (80-.). 309, 548–551 (2005). https://doi.org/10.1126/science.309.5734.548

4. Zweibel, K., Mason, J., Fthenakis, V.: A Solar Grand Plan. Sci. Am. 298, 64–73 (2008). https://doi.org/10.1038/scientificamerican0108-64

5. A.A.M. Sayigh (Eds.): Status of crystalline photovoltaic technology. In: World Renewable Energy Congress VI. Renewables: The Energy for the 21st Century World Renewable Energy Congress VI 1–7 July 2000 Brighton, UK. pp. 2630–2635. Pergamon (2000)

6. John P. Holdren: Science and Technology for Sustainable Well-Being. In: Science. pp. 424–434 (2008)

7. Ipcc: Climate Change 2007: Impacts, Adaptation and Vulnerability. Int. J. Climatol. 976 (2007). https://doi.org/10.2134/jeq2008.0015br

8. Li, G., Jiang, K.J., Li, Y.F., Li, S.L., Yang, L.M.: Efficient structural modification of triphenylamine-based organic dyes for dye-sensitized solar cells. J. Phys. Chem. C. 112, 11591–11599 (2008). https://doi.org/10.1021/jp802436v

9. Jacquemin, D., Preat, J., Wathelet, V., Fontaine, M., Perpète, E.A.: Thioindigo dyes: Highly accurate visible spectra with TD-DFT. J. Am. Chem. Soc. 128, 2072–2083 (2006). https://doi.org/10.1021/ja056676h

10. Jacquemin, D., Wathelet, V., Perpète, E.A., Adamo, C.: Extensive TD-DFT benchmark: Singlet-excited states of organic molecules. J. Chem. Theory Comput. 5, 2420–2435 (2009). https://doi.org/10.1021/ct900298e

11. Sayama, K., Tsukagoshi, S., Hara, K., Ohga, Y., Shinpou, A., Abe, Y., Suga, S., Arakawa, H.: Photoelectrochemical properties of J aggregates of benzothiazole merocyanine dyes on a nanostructured TiO2 film. J. Phys. Chem. B. 106, 1363–1371 (2002). https://doi.org/10.1021/jp0129380

12. Burfeindt, B., Hannappel, T., Storck, W., Willig, F.: Measurement of temperature-independent femtosecond interfacial electron transfer from an anchored molecular electron donor to a semiconductor as acceptor. J. Phys. Chem. 100, 16463–16465 (1996). https://doi.org/10.1021/jp9622905

13. Liu, D., Fessenden, R.W., Hug, G.L., Kamat, P. V: Dye Capped Semiconductor Nanoclusters. Role of Back Electron Transfer in the Photosensitization of SnO2

Nanocrystallites with Cresyl Violet Aggregates. J. Phys. Chem. B. 101, 2583–2590 (1997). https://doi.org/10.1021/jp962695p

14. Hagberg, D.P., Marinado, T., Karlsson, K.M., Nonomura, K., Qin, P., Boschloo, G., Brinck, T., Hagfeldt, A., Sun, L.: Tuning the HOMO and LUMO energy levels of organic chromophores for dye sensitized solar cells. J. Org. Chem. 72, 9550–9556 (2007). https://doi.org/10.1021/jo701592x

15. Bignozzi, C.A., Caramori, S., Cristino, V., Boaretto, R., Argazzi, R., Di Carlo, A.: New components for dye-sensitized Solar Cells. Int. J. Photoenergy. 2010, (2010). https://doi.org/10.1155/2010/458614

16. Snaith, H.J.: Estimating the maximum attainable efficiency in Dye-sensitized solar cells. Adv. Funct. Mater. 20, 13–19 (2010). https://doi.org/10.1002/adfm.200901476

17. Chen, Z., Li, F., Huang, C.: Organic D- -A Dyes for Dye-Sensitized Solar Cell. 1241–1258 (2007)

18. Van Loon, E., Stroosnijder, L.: Evidences of hot excited state electron injection from sensitizer molecules to TiO2 nanocrystalline thin films. Res. Chem. Intermed. 27, 393–406 (2001). https://doi.org/10.1163/156856701104202255

19. Grimme, S., Neese, F.: Double-hybrid density functional theory for excited electronic states of molecules. J. Chem. Phys. 127, (2007). https://doi.org/10.1063/1.2772854

20. Placke, C.: Handout Vortrag 2PPE. 42, (2018). https://doi.org/10.1021/ar900099h

21. Labat, F., Ciofini, I., Adamo, C.: Modeling ZnO phases using a periodic approach: From bulk to surface and beyond. J. Chem. Phys. 131, (2009). https://doi.org/10.1063/1.3179752

22. Tawada, Y., Tsuneda, T., Yanagisawa, S., Yanai, T., Hirao, K.: A long-range-corrected time-dependent density functional theory. J. Chem. Phys. 120, 8425–8433 (2004). https://doi.org/10.1063/1.1688752

23. Baerends, E.J., Ricciardi, G., Rosa, A., Van Gisbergen, S.J.A.: A DFT/TDDFT interpretation of the ground and excited states of porphyrin and porphyrazine complexes. Coord. Chem. Rev. 230, 5–27 (2002). https://doi.org/10.1016/S0010-8545(02)00093-0

24. Adam, W., Krebs, O.: The Nitroso Ene Reaction: A Regioselective and Stereoselective Allylic Nitrogen Functionalization of Mechanistic Delight and Synthetic Potential. Chem. Rev. 103, 4131–4146 (2003). https://doi.org/10.1021/cr030004x

25. Cossi, M., Barone, V.: Time-dependent density functional theory for molecules in liquid solutions. J. Chem. Phys. 115, 4708–4717 (2001). https://doi.org/10.1063/1.1394921

26. Adamo, C., Barone, V.: A TDDFT study of the electronic spectrum of s-tetrazine in

the gas-phase and in aqueous solution. Chem. Phys. Lett. 330, 152–160 (2000). https://doi.org/10.1016/S0009-2614(00)01082-4

27. Preat, J., Jacquemin, D., Wathelet, V., André, J.M., Perpète, E.A.: TD-DFT investigation of the UV spectra of pyranone derivatives. J. Phys. Chem. A. 110, 8144–8150 (2006). https://doi.org/10.1021/jp061260r

28. Chen, K., Costas, M., Kim, J., Tipton, A.K., Que, L.: Olefin cis-dihydroxylation versus epoxidation by non-heme iron catalysts: Two faces of an FeIII-OOH coin. J. Am. Chem. Soc. 124, 3026–3035 (2002). https://doi.org/10.1021/ja0120025

29. Kamiya, M., Sekino, H., Tsuneda, T., Hirao, K.: Nonlinear optical property calculations by the long-range-corrected coupled-perturbed Kohn-Sham method. J. Chem. Phys. 122, (2005). https://doi.org/10.1063/1.1935514

30. Iwashina, T.: The structure and distribution of the flavonoids in plants. J. Plant Res. 113, 287–299 (2000)

31. Regan, B.O., Gratzelt, M.: in The Study of Fast Processes and Transient Species by Electron Pulse Radiolysis. 353, 737–740 (1991). https://doi.org/10.1038/353737a0

32. Zhang, S., Jin, J., Li, D., Fu, Z., Gao, S., Cheng, S.: Increased power conversion e ffi ciency of dye- sensitized solar cells with counter electrodes based. 22092–22100 (2019). https://doi.org/10.1039/c9ra03344k

33. Wang, Z., Ju, M.G., Liang, W.Z.: Electronic excitation and injection of Ru-N3 dye anchored to TiO2 surface. Comput. Theor. Chem. 1097, 8–14 (2016). https://doi.org/10.1016/j.comptc.2016.10.006

34. Sanchez-Bojorge, N.A., Rodriguez-Valdez, L.M., Glossman-Mitnik, D., Flores-Holguin, N.: Theoretical calculation of the maximum absorption wavelength for Cyanidin molecules with several methodologies. Comput. Theor. Chem. 1067, 129–134 (2015). https://doi.org/10.1016/j.comptc.2015.06.002

35. Frau, J., Muñoz, F., Glossman-mitnik, D.: A comparison of the Minnesota family of density functionals for the calculation of conceptual DFT descriptors : citrus flavonoids as a test case. 7, 46–58 (2017)

36. Lakshmanakumar, M., Sriram, S., Balamurugan, D.: Performance analysis of TiO 2 -flavylium compound-based dye-sensitized solar cell (DSSC): a DFT–TDDFT approach. J. Comput. Electron. 17, 1143–1152 (2018). https://doi.org/10.1007/s10825-018-1189-6

37. Sinopoli, A., Citro, I., Calogero, G., Bartolotta, A.: Combined experimental and DFT-TDDFT investigation on anthocyanidins for application in dye-sensitised solar cells. Dye. Pigment. 143, 291–300 (2017). https://doi.org/10.1016/j.dyepig.2017.04.018

38. Knorr, F.J., McHale, J.L., Clark, A.E., Marchioro, A., Moser, J.E.: Dynamics of Interfacial Electron Transfer from Betanin to Nanocrystalline TiO<inf>2</inf>: The Pursuit of Two-Electron Injection. J. Phys. Chem. C. 119, 19030–19041 (2015). https://doi.org/10.1021/acs.jpcc.5b05896

39. Eka, C.P., Brian, Y., Suyatman, Hermawan, K.D.: Donor-modified anthocyanin dye-sensitized solar cell with TiO2 nanoparticles: Density functional theory investigation. Mater. Sci. Forum. 889 MSF, 178–183 (2017). https://doi.org/10.4028/www.scientific.net/MSF.889.178

40. Katoh, R.: Quantitative evaluation of electron injection efficiency in dye-sensitized TiO2 films. Ambio. 41, 143–148 (2012). https://doi.org/10.1007/s13280-012-0277-2

41. Akin, S., Açikgöz, S., Gülen, M., Akyürek, C., Sönmezoğlu, S.: Investigation of the photoinduced electron injection processes for natural dye-sensitized solar cells: The impact of anchoring groups. RSC Adv. 6, 85125–85134 (2016). https://doi.org/10.1039/c6ra19653e

42. Preat, J.: Photoinduced energy-transfer and electron-transfer processes in dye-sensitized solar cells: TDDFT insights for triphenylamine dyes. J. Phys. Chem. C. 114, 16716–16725 (2010). https://doi.org/10.1021/jp1050035

43. Ramachandran K.I; Deepa G.; Namboori K.: Computational Chemistry and Molecular Modeling: Principles and Application. Springer-Verlag Berlin Heidelberg (2008)

44. Frank Jensen: Introduction to Computational Chemistry. (2007)

45. Ben S. Freiser: Organometallic Ion Chemistry. (1995)

46. Tsuneda, T.: Density Functional Theory in Quantum Chemistry.

47. Krishnan, R., Binkley, J.S., Seeger, R., Pople, J.A., Krishnan, R., Binkley, J.S., Seeger, R., Pople, J.A.: Selfconsistent molecular orbital methods . XX . A basis set for correlated wave functions Self-consistent molecular orbital methods . XX . A basis set for correlated wave functions. 650, (1980). https://doi.org/10.1063/1.438955

48. Cramer, C.J.: Essentials of Computational Chemistry: Theories and Models. John Wiley & Sons Ltd (2004)

49. Lewars, E.: Computational Chemistry: Introduction to the Theory and Applications of Molecular and Quantum Mechanics. Kluwer Academic Publisher (2003)

50. Pearson, R.G.: Absolute electronegativity and hardness correlated with molecular orbital theory. 83, 8440–8441 (1986)

51. Parr, R.G., Donnelly, R.A., Levy, M., Palke, W.E.: Electronegativity : The density functional viewpoint. 3801, (1978). https://doi.org/10.1063/1.436185

52. Marcus, R. a.: Electron Transfer Reactions in Chemistry: Theory and Experiment (Nobel Lecture). Angew. Chem. Int. Ed. 32, 1111–1121 (1993). https://doi.org/10.1002/anie.199311113

53. Pourtois, G., Beljonne, D., Cornil, J., Ratner, M.A., Brdas, J.L.: Photoinduced Electron-Transfer Processes along Molecular Wires Based on Phenylenevinylene Oligomers : A Quantum-Chemical Insight Photoinduced Electron-Transfer

Processes along Molecular Wires Based on Phenylenevinylene Oligomers : A Quantum-Chemical Insig. Science (80-.). 1, 4436–4447 (2002). https://doi.org/10.1021/ja017150

54. Fitri, A., Benjelloun, A.T., Benzakour, M., McHarfi, M., Hamidi, M., Bouachrine, M.: Theoretical design of thiazolothiazole-based organic dyes with different electron donors for dye-sensitized solar cells. Spectrochim. Acta - Part A Mol. Biomol. Spectrosc. 132, 232–238 (2014). https://doi.org/10.1016/j.saa.2014.04.164

55. Ding, W.L., Wang, D.M., Geng, Z.Y., Zhao, X.L., Xu, W.B.: Density functional theory characterization and verification of high-performance indoline dyes with D-A-π-A architecture for dye-sensitized solar cells. Dye. Pigment. 98, 125–135 (2013). https://doi.org/10.1016/j.dyepig.2013.02.008

56. Hsu, C.: The Electronic Couplings in Electron Transfer. Acc. Chem. Res. 42, 509–518 (2009). https://doi.org/10.1021/ar800153f

57. Katoh, R., Furube, A., Yoshihara, T., Hara, K., Fujihashi, G., Takano, S., Murata, S., Arakawa, H., Tachiya, M.: Efficiencies of Electron Injection from Excited N3 Dye into Nanocrystalline Semiconductor (ZrO_2, TiO_2, ZnO, Nb_2O_5, SnO_2, In_2O_3) Films. J. Phys. Chem. B. 108, 4818–4822 (2004). https://doi.org/10.1021/jp031260g

58. Fan, W.: Incorporation of Thiadiazole Derivatives as π-Spacer to Construct Efficient Metal-free Organic Dye Sensitizers for Dye-sensitized Solar Cells: A Theoretical Study. Commun. Comput. Chem. 1, 152–170 (2013). https://doi.org/10.4208/cicc.2013.v1.n2.6

59. Zhang, Z.L., Zou, L.Y., Ren, A.M., Liu, Y.F., Feng, J.K., Sun, C.C.: Theoretical studies on the electronic structures and optical properties of star-shaped triazatruxene/heterofluorene co-polymers. Dye. Pigment. 96, 349–363 (2013). https://doi.org/10.1016/j.dyepig.2012.08.020

60. Sang-Aroon, W., Saekow, S., Amornkitbamrung, V.: Density functional theory study on the electronic structure of Monascus dyes as photosensitizer for dye-sensitized solar cells. J. Photochem. Photobiol. A Chem. 236, 35–40 (2012). https://doi.org/10.1016/j.jphotochem.2012.03.014

61. Tian, H., Yang, X., Pan, J., Chen, R., Liu, M., Zhang, Q., Hagfeldt, A., Sun, L.: A triphenylamine dye model for the study of intramolecular energy transfer and charge transfer in dye-sensitized solar cells. Adv. Funct. Mater. 18, 3461–3468 (2008). https://doi.org/10.1002/adfm.200800516

62. Matthews, D., Infelta, P., Grätzel, M.: Calculation of the photocurrent-potential characteristic for regenerative, sensitized semiconductor electrodes. Sol. Energy Mater. Sol. Cells. 44, 119–155 (1996). https://doi.org/10.1016/0927-0248(96)00036-0

63. Tanaka, Y., Ohmiya, A.: Seeing is believing : engineering anthocyanin and carotenoid biosynthetic pathways. https://doi.org/10.1016/j.copbio.2008.02.015

64. Koes, R., Verweij, W., Quattrocchio, F.: Flavonoids : a colorful model for the regulation and evolution of biochemical pathways. 10, (2005). https://doi.org/10.1016/j.tplants.2005.03.002

65. Radfar, M., Sudarshana, M.S., Niranjan, M.H.: Betalains from stem callus cultures of Zaleya decandra L . N . Burm . f . - A medicinal herb. 6, 2443–2447 (2012). https://doi.org/10.5897/JMPR11.1509

66. International, S., Ag, P., Nature, S., Hussain, A.: Sources of Betalains. 15–32 (1900). https://doi.org/10.1007/978-3-319-95624-4

67. Frisch, M.J., Trucks, G.W., Schlegel, H.B., Scuseria, G.E., Robb, M.A., Cheeseman, J.R., Scalmani, G., Barone, V., Mennucci, B., Petersson, G.A., Nakatsuji, H., Caricato, M., Li, X., Hratchian, H.P., Izmaylov, A.F., Bloino, J., Zheng, G., Sonnenberg, J.L., Hada, M., Ehara, M., Toyota, K., Fukuda, R., Hasegawa, J., Ishida, M., Nakajima, T., Honda, Y., Kitao, O., Nakai, H., Vreven, T., Montgomery, J.A., Peralta, J.E., Ogliaro, F., Bearpark, M., Heyd, J.J., Brothers, E., Kudin, K.N., Staroverov, V.N., Keith, T., Kobayashi, R., Normand, J., Raghavachari, K., Rendell, A., Burant, J.C., Iyengar, S.S., Tomasi, J., Cossi, M., Rega, N., Millam, J.M., Klene, M., Knox, J.E., Cross, J.B., Bakken, V., Adamo, C., Jaramillo, J., Gomperts, R., Stratmann, R.E., Yazyev, O., Austin, A.J., Cammi, R., Pomelli, C., Ochterski, J.W., Martin, R.L., Morokuma, K., Zakrzewski, V.G., Voth, G.A., Salvador, P., Dannenberg, J.J., Dapprich, S., Daniels, A.D., Farkas, O., Foresman, J.B., Ortiz, J. V., Cioslowski, J., Fox, D.J., Montgomery Jr., J.A., Peralta, J.E., Ogliaro, F., Bearpark, M., Heyd, J.J., Brothers, E., Kudin, K.N., Staroverov, V.N., Kobayashi, R., Normand, J., Raghavachari, K., Rendell, A., Burant, J.C., Iyengar, S.S., Tomasi, J., Cossi, M., Rega, N., Millam, J.M., Klene, M., Knox, J.E., Cross, J.B., Bakken, V., Adamo, C., Jaramillo, J., Gomperts, R., Stratmann, R.E., Yazyev, O., Austin, A.J., Cammi, R., Pomelli, C., Ochterski, J.W., Martin, R.L., Morokuma, K., Zakrzewski, V.G., Voth, G.A., Salvador, P., Dannenberg, J.J., Dapprich, S., Daniels, A.D., Farkas, Ö., Foresman, J.B., Ortiz, J. V., Cioslowski, J., Fox, D.J.: Gaussian 09, Revision D.01. Gaussian Inc. 1–20 (2013). https://doi.org/10.1159/000348293

68. Roy Dennington, Todd A. Keith, and J.M.M.: GuassView, Version 5.0, (2016)

69. T Bruhn, A Schaumloffel, Y Hemberger, G.B.: SpecDis Version 1.61. Univ. Wuerzburgy, Ger. (2013)

70. S.I. Gorelsky: SWizard Program, (2013)

71. Smith, T.J.: MOLView: A program for analyzing and displaying atomic structures on the Macintosh personal computer. J. Mol. Graph. 13, 122–125 (1995). https://doi.org/10.1016/0263-7855(94)00019-O

72. Todsen, W.L.: ChemDoodle 6.0. (2014)

73. OriginLab Corporation: Origin(Pro), (2010)

74. Zhao, Y., Truhlar, D.G.: The M06 suite of density functionals for main group thermochemistry , thermochemical kinetics , noncovalent interactions , excited

states , and transition elements : two new functionals and systematic testing of four M06-class functionals and 12 other fun. 215–241 (2008). https://doi.org/10.1007/s00214-007-0310-x

75. Zhao, Y., Truhlar, D.G., Zhao, Y., Truhlar, D.G.: A new local density functional for main-group thermochemistry , transition metal bonding , thermochemical kinetics , and noncovalent interactions A new local density functional for main-group thermochemistry , transition metal bonding , thermochemical kin. 194101, (2006). https://doi.org/10.1063/1.2370993

76. Becke, A.D.: Density-fnnctional exchange-energy approximation with correct asymptotic behaviour. 38, 3098–3100 (1988)

77. Chengteh Lee, Weitao Yang, and R.G.P.: Development of the Colle-Salvetti correlation-energy formular into a functional of the electron density. 37, (1988)

78. Peverati, R., Truhlar, D.G.: Screened-exchange density functionals with broad accuracy for chemistry and solid-state physics. Phys. Chem. Chem. Phys. 14, 16187–16191 (2012). https://doi.org/10.1039/c2cp42576a

79. Krishnan, R., Binkley, J.S., Seeger, R., Pople, J.A.: Self-consistent molecular orbital methods. XX. A basis set for correlated wave functions. J. Chem. Phys. 72, 650–654 (1980). https://doi.org/10.1063/1.438955

80. Jacquemin, D., Perpète, E.A., Scalmani, G., Frisch, M.J., Kobayashi, R., Adamo, C.: Assessment of the efficiency of long-range corrected functionals for some properties of large compounds. J. Chem. Phys. 126, (2007). https://doi.org/10.1063/1.2715573

81. Lila, M.A.: Anthocyanins and Human Health : An In Vitro Investigative Approach. 5, 306–313 (2004)

82. Kathuhiko Ueno and Norio Saito: Cyanidin Bromide Monohydrate (3,5,7,3’,4’-Pentahydroxyflavylium Bromide Monohydrate). Acta Crystallogr. 8, 114–116 (1977)

83. Sakata, K., Saito, N., Honda, T.: Ab initio study of molecular structures and excited states in anthocyanidins. 62, 3721–3731 (2006). https://doi.org/10.1016/j.tet.2006.01.081

84. J.B. Harborne: Spectral Methods of Characterizing Anthocyanins. Biochem. J. (1957)

85. Kim, B.G., Chung, K., Kim, J.: Molecular design principle of all-organic dyes for dye-sensitized solar cells. Chem. - A Eur. J. 19, 5220–5230 (2013). https://doi.org/10.1002/chem.201204343

86. Chaudhri, N., Sawhney, N., Madhusudhan, B., Raghav, A., Sankar, M., Satapathi, S.: Effect of functional groups on sensitization of dye-sensitized solar cells (DSSCs) using free base porphyrins. J. Porphyr. Phthalocyanines. 21, 222–230 (2017). https://doi.org/10.1142/S1088424617500390

87. Juma, J.M., Vuai, S.A.H., Surendra Babu, N.: TD-DFT investigations on optoelectronic properties of fluorescein dye derivatives in dye-sensitized solar cells (DSSCs). Int. J. Photoenergy. 2019, (2019). https://doi.org/10.1155/2019/4616198

88. Li, Y., Mi, L., Wang, H., Li, Y., Liang, J.: Design, electron transfer process, and opto-electronic property of solar cell using triphenylamine-based D-π-A architectures. Materials (Basel). 12, (2019). https://doi.org/10.3390/ma12010193

89. Hua, Y., Wang, H., Zhu, X., Islam, A., Han, L.: New simple panchromatic dyes based on thiadiazolo [3 , 4-c] pyridine unit for dye-sensitized solar cells Dyes and Pigments New simple panchromatic dyes based on thiadiazolo [3 , 4- c] pyridine unit for dye-sensitized solar cells. Dye. Pigment. 102, 196–203 (2014). https://doi.org/10.1016/j.dyepig.2013.11.001

90. Li, M., Kou, L., Diao, L., Zhang, Q., Li, Z., Wu, Q., Lu, W., Pan, D., Wei, Z.: Theoretical Study of WS-9-Based Organic Sensitizers for Unusual Vis/NIR Absorption and Highly Efficient Dye-Sensitized Solar Cells. J. Phys. Chem. C. 119, 9782–9790 (2015). https://doi.org/10.1021/acs.jpcc.5b03667

91. Dong, C., Li, X., Jin, P., Zhao, W., Chu, J., Qi, J.: Intersubunit electron transfer (IET) in quantum dots/graphene complex: What features does IET endow the complex with? J. Phys. Chem. C. 116, 15833–15838 (2012). https://doi.org/10.1021/jp304624y

92. Eriksson, S.K., Josefsson, I., Ellis, H., Amat, A., Pastore, M., Oscarsson, J., Lindblad, R., Eriksson, A.I.K., Johansson, E.M.J., Boschloo, G., Hagfeldt, A., Fantacci, S., Odelius, M., Rensmo, H.: Geometrical and energetical structural changes in organic dyes for dye-sensitized solar cells probed using photoelectron spectroscopy and DFT. Phys. Chem. Chem. Phys. 18, 252–260 (2016). https://doi.org/10.1039/c5cp04589d

APPENDIX

Published Article

Journal of Computational Electronics (2019) 18:396–406
https://doi.org/10.1007/s10825-019-01331-5

Electron injection in anthocyanidin and betalain dyes for dye-sensitized solar cells: a DFT approach

Aanuoluwapo Raphael Obasuyi[1] · Daniel Glossman-Mitnik[1] · Norma Flores-Holguín[1]

Published online: 9 April 2019

Abstract
A theoretical investigation was carried out using density functional theory at the MN12SX/6-311+G(d,p) level of theory to calculate and compare the photoinduced electron injection for selected members of the anthocyanidin and betalain families. The rate constant of the injection for both families was calculated, and it was verified that the regeneration in the dye during the DSSC operation is caused by an energetic electron injection of the matched electrons in the dye. The present research shows that the rate constant of electron injection of the selected anthocyanidin family was very rapid: Aurantinidin has the overall best injection rate for both families. Aromaticity, the open-circuit voltage V_{oc}, the ΔG_{inject} and ΔG_{reg} values for the selected molecule play a vital role in the comparison of both selected families. A prediction of the best dye based on the above properties was made for the maximum efficiency of the DSSC to be achieved.

Keywords Electron injection · Anthocyanidin · Betalain · DFT · DSSC

1 Introduction

Solar photovoltaic devices in the world at large are a promising low-carbon level future technology, and as it stands, a huge increase is on the creation of renewable energy sources due to the energetic and environmental crisis [1–7]. An average value of 10% solar power conversion efficiency (SPCE) has been obtained for ruthenium (Ru) complex photosensitizers, and for the past 20 years, it has been the most widely used category of dyes. The high production cost and the low abundance in nature of Ru-derived sensitizers have been a major drawback for such dyes despite their high SPCE value. Metal-free sensitizers (organic and natural dyes) have been recently considered by researchers as alternative molecules for DSSC operation. Organic dyes have been considered as a substitute for Ru complexes because of their high molar extinction coefficient, low-cost preparation processes and for having less environmental or health issues. Sensitization occurs due to the following:

- The highest occupied molecular orbital (HOMO) must be below the iodine/iodide redox potential; also the energy of the lowest unoccupied molecular orbital (LUMO) needs to be higher than the conduction band edge of the semiconductor.
- For a good photocurrent response, the light-harvesting ability of the dye must be high.
- For a high photoinduced intramolecular charge transfer, the conjugation between the donor and anchoring group needs to remain intact [8–12].

The roadmaps for intramolecular charge transfer and the resulting electron transfer have been theoretically investigated by a lot of quantum chemical techniques. These techniques are very useful tools due to their efficiency in the interpretation of experimental data [13, 14]. Quantum chemical techniques have shown the importance carried by the electronic coupling between the reactants and products (VRP) in the simplification of electron transfer reactions [15–21]. Time-dependent density functional theory (TDDFT) is one of the frequently used approaches for calculating electronic excited states; it normally gives results that agree with experimental data at low computational costs, in particular when hybrid functionals are used [22–31].

In this research, selected members of the anthocyanidin and betalain families were carefully studied and the

✉ Norma Flores-Holguín
norma.flores@cimav.edu.mx

[1] Laboratorio Virtual NANOCOSMOS, Departamento de Medio Ambiente y Energía, Centro de Investigación en Materiales Avanzados, Miguel de Cervantes 120, Complejo Industrial Chihuahua, Chihuahua, Chih 31136, Mexico

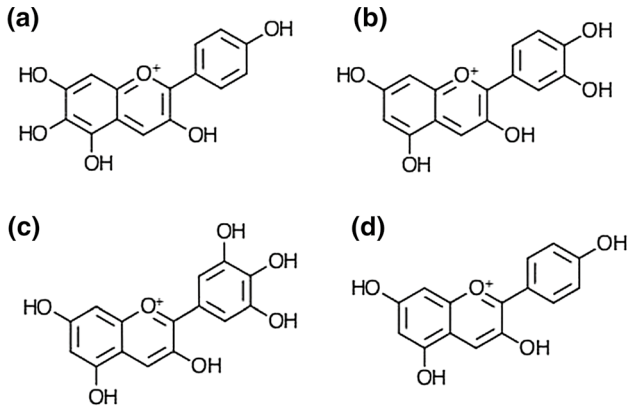

Fig. 1 Schematic structures of selected dyes of the anthocyanidin family: **a** aurantinidin; **b** cyanidin; **c** delphinidin; **d** pelargonidin

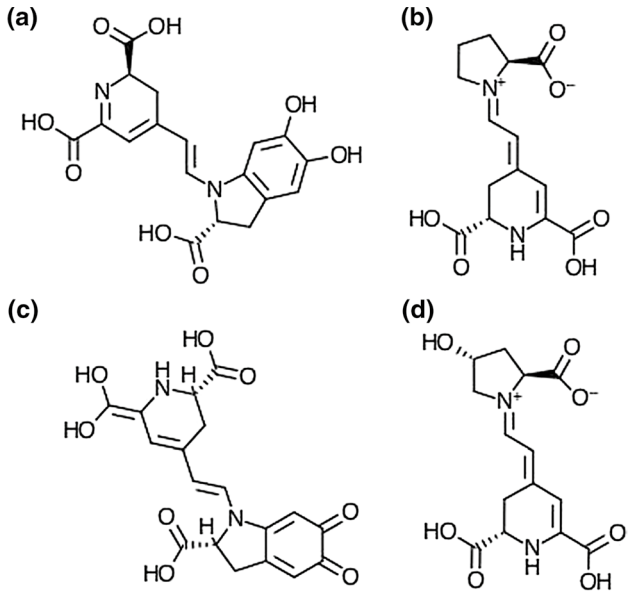

Fig. 2 Schematic structure of selected dyes of the betalain family: **a** betanidin; **b** isobetanidin; **c** indicaxanthin; **d** portulaxanthin

electron transfer properties of these molecules were compared. These dyes families have been successfully proven to show high conversion efficiency in DSSC devices [32, 33] because both molecules possess hole-transporting ability [34].

We report here the theoretical study of some selected dyes of the anthocyanidin and betalain families where the object of this investigation relies on the calculation of the electron injection of the selected dyes families by using a computational procedure that delivers a qualitatively good description of the excited states of the dyes [34–36].

Figures 1 and 2 show the schematic structures of the selected members of the anthocyanidin and betalain families, respectively.

2 Theoretical background

2.1 Electron transfer

The electron transfer from a dye to a semiconductor and the rate of the charge transfer process can be derived from Marcus theory [37–39] as:

$$k_{\text{inject}} = \left(\frac{\pi}{\hbar\lambda k_{\text{B}}T}\right)^{0.5} |V_{\text{RP}}|^2 e^{\left(\frac{-(\Delta G_{\text{inject}}+\lambda)^2}{4\lambda k_{\text{B}}T}\right)} \quad (1)$$

In Eq. 1, k_{inject} is the rate constant (in s^{-1}) of the electron injection from the dye to TiO_2: the higher the electron injection, the best the SPCE factor achieved and more efficient is the DSSC. $K_{\text{B}}T$ is the Boltzmann thermal energy, $\hbar = h/2\pi$ is related to the Planck constant, ΔG_{inject} is the free energy of injection, and λ is the reorganization energy of the system.

2.2 Reorganization energy

The reorganization energy is the energy required to move from the ground state to the excited state without electrons being transferred. The reorganization energy λ can be separated into the sum of two primary components:

1. the hole reorganization energy λ_{h}, and
2. the electron reorganization energy λ_{e}.

The total reorganization energy (λ) could help in enhancing the Jsc, while a lower value of λ can accelerate the rate of the charge-carrier transport. The total reorganization energy (λ) is calculated using the following equation [40, 41]:

$$\lambda = \lambda_{\text{h}} + \lambda_{\text{e}}$$

with

$$\lambda_{\text{h}} = (E_0^+ - E_+^+) + (E_+^0 - E_0^0)$$
$$\lambda_{\text{e}} = (E_0^- - E_-^-) + (E_-^0 - E_0^0)$$

where E_0^+ (E_0^-) is the energy of the cation (anion) calculated at the optimized structure of the neutral molecule. Similarly, E_+^+ (E_-^-) is the energy of the cation (anion) calculated with the optimized cation (anion) structure, and E_+^0 (E_-^0) is the energy of the neutral molecule calculated at the cationic (anionic) state. Finally, E_0^0 is the energy of the neutral molecule at the ground state.

2.3 Coupling constant

The coupling constant between the reagent and the product potential curves is denoted by $|V_{\text{RP}}|$. A high value of $|V_{\text{RP}}|$

leads to higher injection time, and a high value of $|V_{RP}|$ will give a better result for the sensitizer, the best SPCE factor and the most efficient DSSC [39, 42]. Hsu et al. [42] explained that $|V_{RP}|$ can be evaluated as:

$$|V_{RP}| = \frac{\Delta E_{RP}}{2} \tag{2}$$

2.4 Energy difference

The energy difference can be formally expressed within Koopmans approximation as:

$$\Delta E_{RP} = [E^{dye}_{LUMO} + 2E^{dye}_{HOMO}] - [E^{dye}_{LUMO} + E^{dye}_{HOMO} + E^{TiO_2}_{CB}] \tag{3}$$

where $E^{TiO_2}_{CB}$ is the conduction band edge. Though it is often difficult to accurately determine $E^{TiO_2}_{CB}$ because it is highly sensitive to the conditions like pH of the solution, we have decided to use $E^{TiO_2}_{CB} = -4.0$ eV, which is the experimental value corresponding to the conditions where the semiconductor is in contact with aqueous redox electrolytes of fixed pH 7.0 [43]. In a closed-shell system the HOMO energy is related to the potential of first oxidation (i.e., $-E^{dye}_{HOMO} = E^{dye}_{ox}$). As a result, Eq. 3 becomes

$$\Delta E_{RP} = -[E^{dye}_{ox} + E^{TiO_2}_{CB}] \tag{4}$$

2.5 Free energy change

The free energy change (eV) for the electron injection can be expressed as [43]:

$$\Delta G_{inject} = E^{dye*}_{ox} - E^{TiO_2}_{CB} \tag{5}$$

When the entropic component can be neglected in the calculation of the injection energetic balance, ΔE_{RP} corresponds to the injection free energy change ΔG_{inject}, where E^{dye*}_{ox} is the oxidation potential of the dye in the excited state, and $E^{TiO_2}_{CB}$ is the reduction potential of the semiconductor conduction band. For this reaction path, the excited-state oxidation potential can be extracted from the redox potential of the ground state, E^{dye}_{ox}, which has been calculated at the MN12SX/6-311+G(d,p) level of theory approach and the vertical transition energy corresponding to the photoinduced intramolecular charge transfer (ICT),

$$E^{dye*}_{ox} = E^{dye}_{ox} - \lambda^{ICT}_{max} \tag{6}$$

where λ^{ICT}_{max} is the energy of the ICT. It must be noted that this relation is only valid if the entropy change during the light absorption process can be neglected.

2.6 Dye regeneration energy

The dye regeneration energy ΔG_{reg} is an essential factor that determines the rate of dye recombination: a negative value of ΔG_{reg} implies a low dye recombination, and a low dye recombination increases the rate of electron injection in the dye [44]. The dye regeneration ΔG_{reg} can be calculated by using Eq. 7:

$$\Delta G_{reg} = E^{dye}_{ox} + E^{electrolyte}_{redox} \tag{7}$$

where $E^{electrolyte}_{redox}$ is the electrolyte redox potential (−4.85 eV) [45].

It has been reported that an insufficient driving force for dye regeneration causes a low open-circuit voltage (V_{OC}) and poor photocurrent generation, because of fast recombination between the injected electrons and the photooxidized dye molecules [46].

The photooxidized dye should also be regenerated rapidly to avoid charge recombination between the hole on the oxidized dye and the injected electron to the electrode and to minimize chemical degradation during the DSSC operation cycle.

2.7 Light-harvesting efficiency

Light-harvesting efficiency is the fraction of light intensity absorbed by the dye at a certain wavelength in the DSSC. The light-harvesting efficiency (LHE) of the dye has to be as high as possible to maximize the photocurrent response. LHE is expressed as [47]:

$$LHE = 1 - 10^{-A} = 1 - 10^{-f} \tag{8}$$

where $A(f)$ is the absorption (oscillator strength) of the dye associated with the λ^{ICT}_{max}.

2.8 Open-circuit voltage

The open-circuit voltage V_{OC} is the electron injection from the E_{LUMO} of the dye to the conduction band (ECB) of TiO_2 (101) anatase phase semiconductor surface. V_{OC} (eV) can be calculated using [48]:

$$V_{OC} = E_{LUMO} - E_{CB} \tag{9}$$

2.9 Electron transfer: Helmholtz potential function

It has been proved that Eq. 1 provides a low injection rate for systems with enough relaxation time after electronic excitation. It has been noted that Marcus theory gives a good result at low potentials, but at high potentials, the result is very low [34].

For a high potential to be achieved, E_0 must be greater than the reorganizing energy λ, where E_0 is the ground rotation–vibration state. E_0 can be calculated using the following formula [34]:

$$E_0 - E_{CB} = \Delta G_{inject} + \lambda$$

We can conclude that the rate constant and $ki_{inject}$are very low when using Eq. 1. According to previous research, electron injection is necessary to take place into the conduction band of semiconductor from the dye in the range of pico- or femtoseconds [46]. Also, it has been noted that errors with Eq. 1 calculations are attributed to:

1. The large uncertainty concerning the conformational space of the systems.
2. The error related to the different key parameters combined to the high numerical sensitivity of the exponential function.
3. The dye molecules are probably overestimated by the DFT analysis [34].

Due to these justifications, a more redefined formula was derived from Helmholtz potential function, as shown below in Eq. 10:

$$k_{inject} = \left(\frac{\pi}{\hbar^2 k_B T}\right)^{0.5} |V_{RP}|[-\Delta G_{inject} - (E_{CB} - E_F - \lambda)]^{0.5} \quad (10)$$

where $E_{CB} - E_F$ is the difference between the energy of the conduction band and the energy of the Fermi level for TiO_2, and this difference is 1.6 eV [34]. Equation 10 delivers an almost linear dependence of the rate constant on the free energy of injection at high potential. By using Eq. 10, one can calculate a rate constant which is more realistic for the injection process.

3 Settings and computational details

All calculations have been performed with the Gaussian 09 package [49]. The MN12SX functional [50] and the 6-311+G(d,p) basis set [51] were used for the analysis of the selected anthocyanidin and betalain family dyes. This basis set has been chosen because it has been shown that return a converged λ_{max} for a series of calculations, while a smaller basis set would give a too short λ_{max} (in nm) [36].

The MN12SX functional belongs to the Minnesota family which is characterized by all parameterization against a broad range of chemical data. It belongs to the non-separable gradient approximation functionals that include exchange and correlation in the form of a non-separable gradient improvement of uniform electron gas exchange. Particularly, MN12SX was constructed adding both, kinetic energy density and screened exchange. The functional coefficients were optimized on a training of 369 chemistry and physics data, both chemistry energetic and structural data. The performance of the functional was probed on a set of databases, and results show that the functional provides broadly accurate performance for all chemistry and solid-state physics databases considered and has an excellent performance for chemistry and physics and for energies and structures [50].

3.1 Convergence thresholds

The convergence criteria used in this work are the default for Gaussian 09. The maximum component of the force must be below the cutoff value of 0.0045. This means that the molecule is at the state of a local minimum or a local maximum. The root-mean-square must be 0, but the cutoff is 0.0003. Teh calculated displacement for the next step has a cutoff of 0.0018 and the cutoff for root-mean-square of the displacement is 0.0012. All these values are interpreted as 0 by the Gaussian program. For energy calculations, the requested convergence is 1.00D-08.

4 Results and discussion

4.1 Geometry optimization

The optimizations of the molecules were performed for the selected dyes of the anthocyanidin and betalain families. For the anthocyanidin family, the considered dyes are aurantinidin, cyanidin, delphinidin and pelargonidin, which were selected because they have a similar orientation of the radical atoms of either −H or −OH. The betalain family was carefully analyzed, from the two classes of betalain, which are betacyanins and betaxanthins, two dyes were considered from each class. For the betacyanin class, we considered the aglycone nature of the selected dyes, which are betanidin and isobetanidin, while that for betaxanthins, we considered indicaxanthin and portulaxanthin. The geometry optimizations were performed with DFT level using the MN12SX/6-311+G(d,p) level of theory.

After the optimization of all the selected dyes was completed, the molecular structures were not twisted and they all stay flat. The presence of the hydroxyl in all the molecules helps in the non-twisting ability, thereby making the molecules to be flat. A non-overlap of atoms of a molecule produces a better overall conversion efficiency [44], which makes this a good dye for a DSSC.

4.2 Molecular orbitals

The driving force for the electron injection from a dye to a semiconductor oxide is the energy-level difference between

the LUMO of the dye and the E_{CB} of the oxide. However, explaining the electron-injection efficiency only with the required energy level of the dyes is not enough, because the degree of electron injection is also strongly affected by the molecular orientation and spatial arrangement of them, such as aggregation and electronic coupling with the electrode [52].

Organic dyes' intrinsic properties, such as shape, geometry and conjugation length, should also be considered in the dye design to improve the electron-injection efficiency. As shown in Figs. 3 and 4, for the HOMO the electron density is mostly localized around the electron-donating group. However, for the LUMO the electron density is localized near the electron-withdrawing acceptor side. This indicates that the electrons would move from the donor to the acceptor after the light absorption through excitation, and the structure is advantageous to direct intramolecular electron transfer from donor to acceptor.

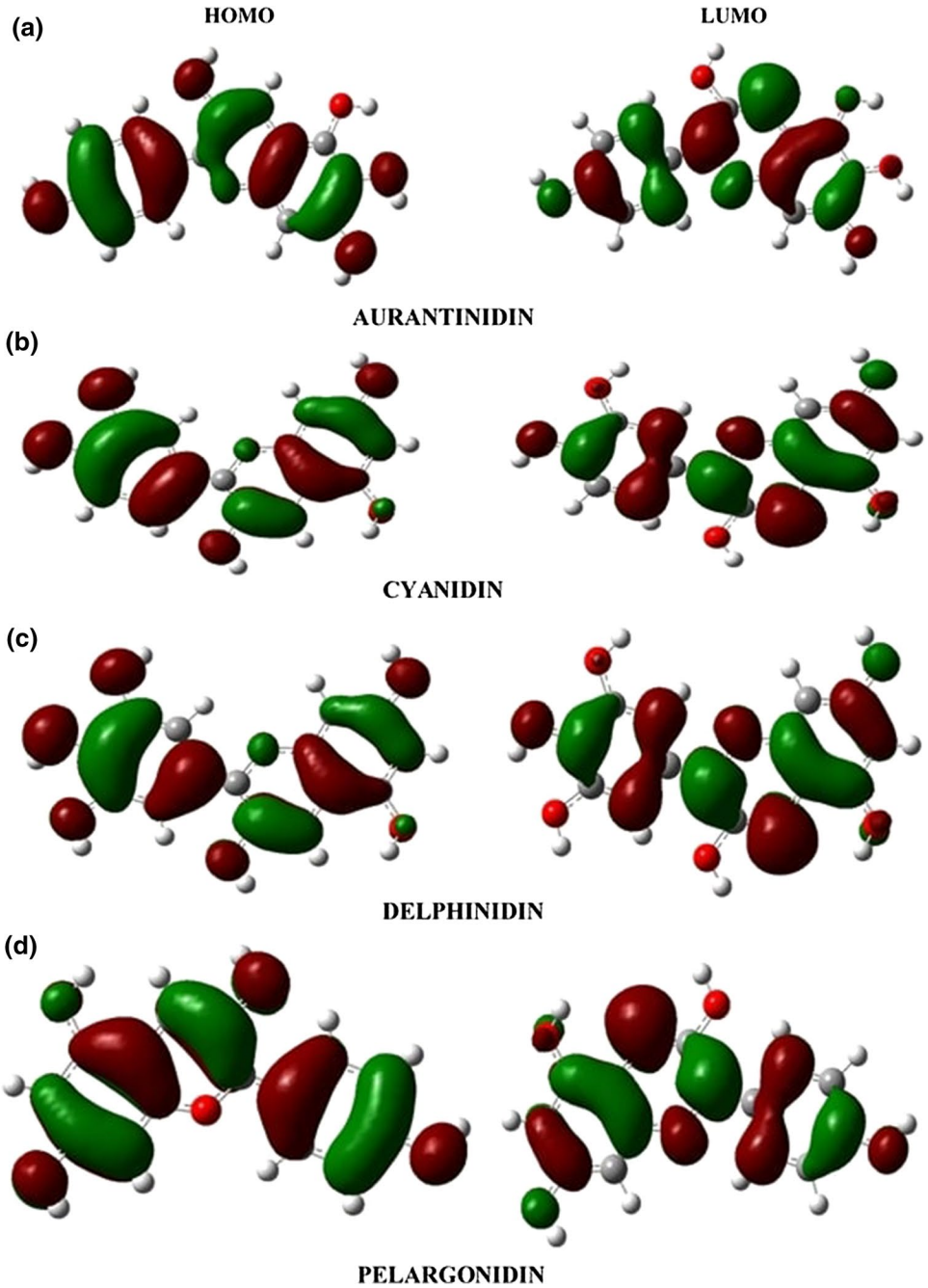

Fig. 3 Optimized molecular structures of selected dyes of the anthocyanidin family: **a** aurantinidin; **b** cyanidin; **c** delphinidin; **d** pelargonidin

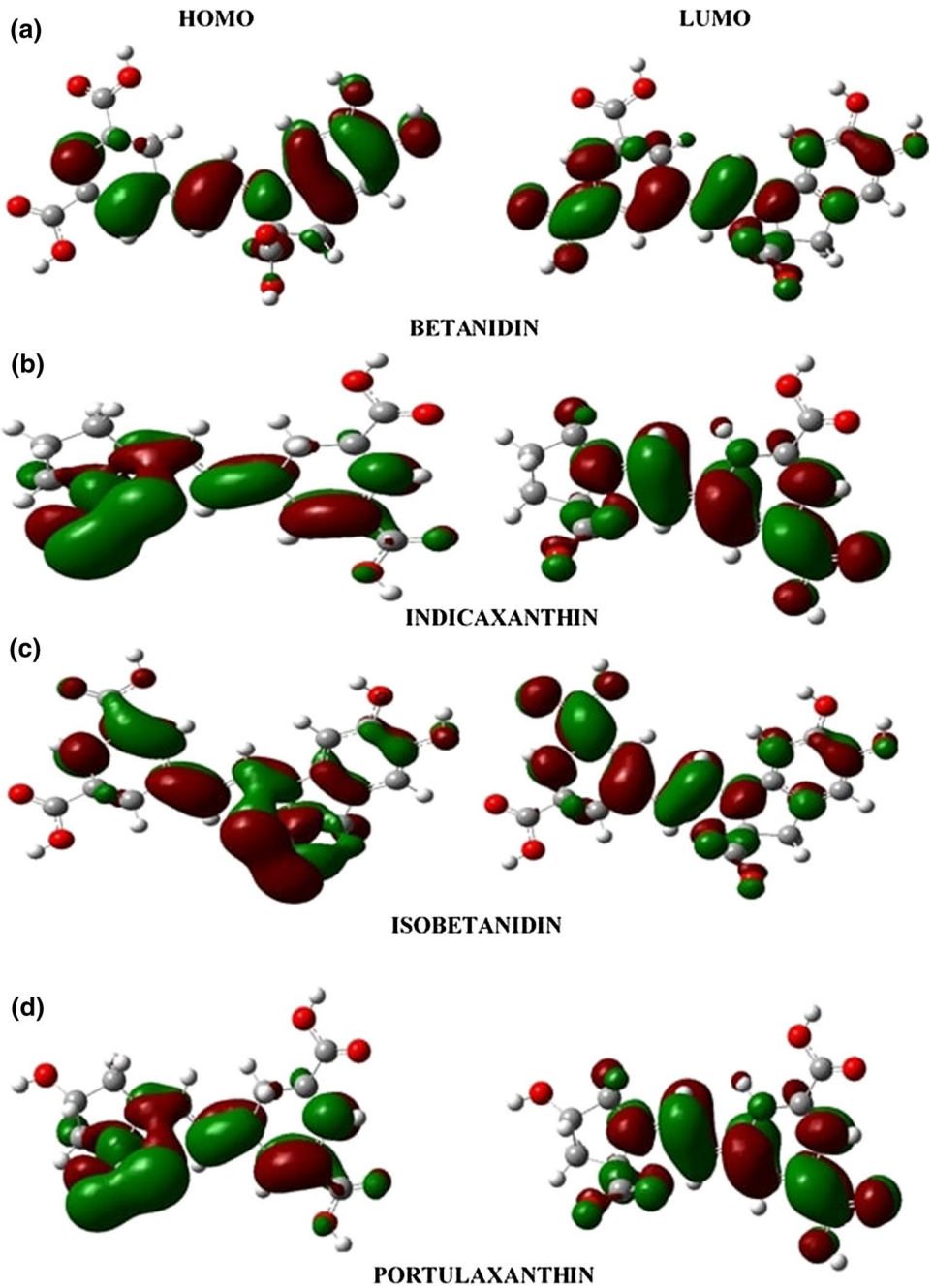

Fig. 4 Optimized molecular structures of selected dyes of the betalain family: **a** betanidin; **b** isobetanidin; **c** indicaxanthin; **d** portulaxanthin

4.3 Optical properties

The excited-state transitions computed at the MN12SX/6-311+G(d,p) level of theory can be classified according to the occupied and unoccupied MOs combinations. The computed UV-visible absorption data of the selected dyes of the anthocyanidin and betalain families in the gas phase are shown in Tables 1 and 2, respectively. The absorption spectra of the selected dyes were compared among them. Within the investigated visible absorption spectrum range of 400–600 nm, they all show maxima peaks.

For the MN12SX/6-311+G(d,p) level of theory in the gas phase, the highest oscillator strengths are 0.2302, 0.2403, 0.1059 and 0.1339 for aurantinidin, cyanidin, delphinidin and pelargonidin, respectively. All the molecules have the highest oscillator strength transition at the HOMO–LUMO level. Also, for the betalain family, using MN12SX/6-311+G(d,p) level of theory, they have the highest oscillator strengths at 0.2762, 0.2587, 0.1673 and 0.2402 for betanidin, indicaxanthin, isobetanidin and portulaxanthin, respectively, at the HOMO–LUMO level. It is also noted that betaxanthins (indicaxanthin and portulaxanthin) have relative lower

Table 1 Absorption wavelength (nm) energy levels of HOMO and LUMO and oscillator strengths for the selected dyes of the anthocyanin family in the gas phase calculated at the MN12SX/6-311+G(d,p) level of theory

Dyes	λ (nm)	f	Transition (%)
Aurantinidin	556.0	0.2302	H-L (84)
	488.7	0.0783	H-L (73)
			H-L+1 (12)
	447.4	0.1457	H-L+1 (47)
	424.8	0.0077	H-L +1(24)
	401.0	0.0343	H-L (63)
Cyanidin	558.5	0.2403	H-L (91)
	498.4	0.0556	H-L (78)
	464.5	0.1364	H-L (76)
	446.3	0.0875	H-L (65)
			H-L+1 (13)
	425.8	0.0674	H-L+1 (55)
	410.6	0.0986	H-L (60)
Delphinidin	563.6	0.1059	H-L (85)
	496.1	0.0896	H-L (64)
	466.6	0.0743	H-L+1 (54)
	448.3	0.0405	H-L (59)
			H-L+1 (24)
Pelargonidin	536.7	0.1339	H-L (96)
	489.5	0.0856	H-L (65)
	465.0	0.0494	H-L+1 (21)
	435.1	0.0358	H-L+1 (26)

Table 2 Absorption wavelength (nm) energy levels of HOMO and LUMO and oscillator strengths for the selected dyes of the betalain family in the gas phase calculated at the MN12SX/6-311+G(d,p) level of theory

Dyes	λ (nm)	f	Transition (%)
Betanidin	530.2	0.2762	H-L (88)
	484.5	0.1895	H-L+2 (55)
	442.4	0.6264	H-L+2 (23)
	402.0	0.0067	H-L (80)
			H-L+1 (37)
Indicaxanthin	532.1	0.2587	H-L (80)
	484.2	0.0683	H-L+1 (54)
	454.1	0.1324	H-L+2 (45)
	428.3	0.0173	H-L (74)
Isobetanidin	518.8	0.1673	H-L (92)
	469.2	0.0548	H-L+2 (45)
	426.7	0.0384	H-L+1 (63)
	403.1	0.0145	H-L (69)
			H-L+1 (24)
Portulaxanthin	508.1	0.2402	H-L (86)
	472.5	0.1474	H-L+1 (67)
	455.2	0.0342	H-L+2 (25)
	406.7	0.0195	H-L+1 (59)

Table 3 Energy levels for the selected dyes of the anthocyanidin family

Anthocyanidin	HOMO (eV)	LUMO (eV)	HOMO–LUMO gap (eV)
Aurantinidin	− 5.70	− 2.65	3.05
Cyanidin	− 5.64	− 2.55	3.09
Delphinidin	− 5.75	− 2.59	3.16
Pelargonidin	− 5.65	− 2.44	3.21

Table 4 Energy level for the selected dyes of the betalain family

Betalain	HOMO (ev)	LUMO (eV)	HOMO–LUMO gap (eV)
Betanidin	− 6.00	− 2.85	3.15
Isobetanidin	− 7.02	− 3.59	3.43
Indicaxanthin	− 6.97	− 3.55	3.42
Portulaxanthin	− 6.78	− 3.59	3.19

wavelengths compared to all the selected dyes. This can be attributed to the presence of one benzene ring in the betaxanthin family. Benzene ring has aromaticity with π-electrons, and these rings seem to be a factor that increases the wavelength of the molecule with more than one ring.

4.4 Energy band gaps

Tables 3 and 4 show the HOMO, LUMO and energy band gaps for the selected dyes of the anthocyanidin and betalain families, respectively. The LUMO energy values for all dyes are located above the conduction band edge of TiO_2 (− 4.0 eV). Also, the highest occupied molecular orbital (HOMO) energy is below the redox mediator of I^-/I^{3-} (−4.85 eV). The relative matching of the electronic levels of the sensitizers would lead to an energetically favorable electron injection as well as to the regeneration of the oxidized dye during DSSC operation. It was also noted that the energy gap is very close and even some molecules have the same value.

4.5 Electron injection

Tables 5 and 6 show the injection timescale in fs (10^{-16}), k_{inject}, ΔG_{inject}, $E_{\text{ox}}^{\text{dye}}$, $E_{\text{ox}}^{\text{dye*}}$, $E_{\text{ox}}^{\text{dye}}$, $E_{\text{ox}}^{\text{dye}}$, ΔG_{RP}, f, LHE, V_{OC} for the selected dyes of the anthocyanidin and betalain families, respectively. According to previous research, it has been demonstrated that a driving force $-\Delta G_{\text{inject}}$ of 0.20 eV is necessary for efficient dye regeneration. From our results, it was observed that $-\Delta G_{\text{inject}}$ varies in values in the selected anthocyanidin family dyes, ranging from 1.87 to 2.16 eV. Also, the selected betalain family dyes have ΔG_{inject} values

Table 5 Electron injection-related properties for the selected dyes of the anthocyanin family

Anthocyanidin	Injection timescale (fs)	k_{inject}	ΔG_{inject}	E_{ox}^{dye}	E_{ox}^{dye*}	λ_{max}^{ICT}
Aurantinidin	0.0391	2.56×10^{16}	− 2.16	4.07	1.84	2.23
Cyanidin	0.0472	2.12×10^{16}	− 1.92	4.30	2.08	2.22
Delphinidin	0.0531	1.88×10^{16}	− 1.87	4.33	2.13	2.20
Pelargonidin	0.0454	2.20×10^{16}	− 2.03	4.28	1.97	2.31
	V_{RP}	ΔG_{reg}	f	LHE	V_{OC}	
Aurantinidin	1.080	− 0.78	0.2302	0.4114	1.35	
Cyanidin	0.960	− 0.55	0.2463	0.4328	1.45	
Delphinidin	0.935	− 0.52	0.1059	0.2164	1.41	
Pelargonidin	1.015	− 0.57	0.1339	0.2653	1.56	

Table 6 Electron injection-related properties for the selected dyes of the betalain family

Betalain	Injection timescale (fs)	k_{inject}	ΔG_{inject}	E_{ox}^{dye}	E_{ox}^{dye*}	λ_{max}^{ICT}
Betanidin	0.1032	9.69×10^{15}	− 1.10	5.38	2.90	2.48
Isobetanidin	0.1295	7.72×10^{15}	− 0.63	5.70	3.37	2.33
Indicaxanthin	0.1211	8.26×10^{15}	− 0.71	5.68	3.29	2.39
Portulaxanthin	0.1047	9.55×10^{15}	− 0.69	5.75	3.31	2.44
	V_{RP}	ΔG_{reg}	f	LHE	V_{OC}	
Betanidin	0.550	− 0.53	0.2762	0.4706	1.15	
Isobetanidin	0.315	− 0.85	0.2587	0.4488	0.41	
Indicaxanthin	0.355	− 0.83	0.1673	0.3197	0.45	
Portulaxanthin	0.345	− 0.90	0.2402	0.4248	0.41	

ranging from 0.63 to 1.10 eV. The values of ΔG_{inject} for the dyes of the anthocyanidin and betalain families are above the required 0.2 eV for an electron injection to take place, and this means that these values support good electron injection from the dye to the conduction band of the semiconductor materials [53].

From Tables 5 and 6, it can be observed that the ΔG_{inject} values are all negative and this indicates that all the selected dyes have excited states above the conduction band of TiO_2 which will make the dyes to easily inject electrons into the semiconductor materials.

It is also observed from Table 5 that ΔG_{reg} shows negative values for the anthocyanidin family dyes, which is an indication that the redox level of the electrolyte is lower than the ground states of the selected dyes. These particular attributes make the electron recombination to be reduced. On the contrary, by checking Table 6 for selected dyes of the betalain family, positive values for ΔG_{reg} are present, which will make electron recombination to be faster.

Table 5 and 6 show that the rate constant k_{inject} of electron injection is very fast, which implies that the selected dyes of the anthocyanidin and betalain families are good sensitizers for the electron injection into the conduction band of the semiconductor material. However, due to the values of ΔG_{reg} for betalain family dyes, the electron recombination will be higher. Aurantinidin has the highest rate constant of $2.56 \times 10^{16}\ s^{-1}$ in the anthocyanidin family. This indicates that among the selected anthocyanidin family using MN12SX/6-311+G(d,p) level of theory, aurantinidin gives the better electron-injection value among the selected dyes having an injection timescale of 0.0391 fs due to its highest electron-injection value. Another dyes also have good values for the rate constant. Betanidin has the highest rate constant of $9.69 \times 10^{15}\ s^{-1}$ in the betalain family giving a corresponding value of 0.1032 fs in the injection timescale.

Aurantinidin dye will give a good short-circuit current density Jsc because of its relative high LHE and k_{inject}, the higher the open-circuit voltage (V_{OC}) and the best overall efficiency (η). V_{OC} values of this selected dye besides ΔG_{inject} and LHE are also another factor that affects efficiency. Anthocyanidin family dyes give better V_{OC} values. As the consequence of this study of these organic dyes, we could predict that the aurantinidin dye with the large LHE and k_{inject} and a relatively high value of V_{OC} will present the maximum efficiency. The light-harvesting efficiency (LHE) is the efficiency of dye in response to light. It is another

factor which indicates the efficiency of DSSC. The light-harvesting efficiency (LHE) of the dye should be as high as feasible to maximize the photocurrent response.

In this research, it has been discovered that anthocyanidin dyes give better injection ability than those from the betalain family due to its high LHE, k_{inject} and V_{OC}, and this high value can be due to the numbers of benzene rings present in the anthocyanidin family dyes. Benzene ring gives more stability to a molecule due to its aromaticity nature.

5 Conclusions

The electronic structures of the selected dyes of the anthocyanidin and betanidin families were used to calculate their optical properties and energy band gaps. We have calculated the key parameters controlling the intramolecular charge transfer (ICT) injection and ET transfer rate constants.

The results obtained from this research show negative values of ΔG_{inject}. This indicates, according to Lakshmanakumar et al, that the excited state of the dye lies above the conduction band of TiO_2 and will rapidly inject electrons from that excited state into the TiO_2 semiconductor [54]. The values from their studied dyes show also negative numbers for ΔG_{inject} ranging from −1.41 to −2.47 eV. Jin et al. [55] studied the theoretical design of porphyrin sensitized for DSSC applications and got values ranging from − 0.92 to − 1.16 eV.

Also the results show a fast rate constant of electron injection but much lower than the values found by Preat [38] using triphenylamine dyes which reported an injection timescale of 0.21 fs and 0.30 fs.

Anthocyanidin family dyes showed better injection ability compared to the betalain family dyes due to the double aromatic ring they possess. The ΔG_{reg} factor contributed to the low electron injection of betalain family dyes. The light-harvesting efficiency is large enough to maximize the photocurrent response. Finally, this research showed that the aurantinidin dye is the best photosensitizer for DSSC among the selected dyes from both families that have been studied because it has good LHE, ΔG_{inject}, and a relative high V_{OC}.

Acknowledgements Norma Flores-Holguín and Daniel Glossman-Mitnik are CONACyT and CIMAV researchers. Obasuyi Aanuoluwapo Raphael gratefully acknowledges a Doctoral Fellowship from the National Science and Technology Council in Mexico (CONACYT).

References

1. Holdren, J.P.: Science and technology for sustainable well-being. Science **319**(5862), 424–434 (2008)
2. Mackay, A.: Climate change 2007: impacts, adaptation and vulnerability. Contribution of working group II to the fourth assessment report of the intergovernmental panel on climate change. J. Environ. Qual. **37**(6), 2407 (2008)
3. Green, M.A.: Status of crystalline photovoltaic technology (Chapter 579). In: Sayigh, A. (ed.) World Renewable Energy Congress VI, pp. 2630–2635. Pergamon, Oxford (2000)
4. Zweibel, K., Mason, J., Fthenakis, V.: A solar grand plan. Sci. Am. **298**(1), 64–73 (2008)
5. Service, R.F.: Is it time to shoot for the sun? Science **309**(5734), 548–551 (2005)
6. Kammen, D.M., Pacca, S.: Assessing the costs of electricity. Annu. Rev. Environ. Resour. **29**(1), 301–344 (2004)
7. Alsema, E.A.: Energy pay-back time and CO_2 emissions of PV systems. Prog. Photovolt. Res. Appl. **8**(1), 17–25 (2000)
8. Li, G., Jiang, K.J., Li, Y.F., Li, S.L., Yang, L.M.: Efficient structural modification of triphenylamine-based organic dyes for dye-sensitized solar cells. J. Phys. Chem. C **112**(30), 11591–11599 (2008)
9. Sayama, K., Tsukagoshi, S., Hara, K., Ohga, Y., Shinpou, A., Abe, Y., Suga, S., Arakawa, H.: Photoelectrochemical properties of J aggregates of benzothiazole merocyanine dyes on a nanostructured TiO_2 film. J. Phys. Chem. B **106**(6), 1363–1371 (2002)
10. Burfeindt, B., Hannappel, T., Storck, W., Willig, F.: Measurement of temperature-independent femtosecond interfacial electron transfer from an anchored molecular electron donor to a semiconductor as acceptor. J. Phys. Chem. **100**(41), 16463–16465 (1996)
11. Liu, D., Fessenden, R.W., Hug, G.L., Kamat, P.V.: Dye capped semiconductor nanoclusters. Role of back electron transfer in the photosensitization of SnO_2 nanocrystallites with cresyl violet aggregates. J. Phys. Chem. B **101**(14), 2583–2590 (1997)
12. Hagberg, D.P., Marinado, T., Karlsson, K.M., Nonomura, K., Qin, P., Boschloo, G., Brinck, T., Hagfeldt, A., Sun, L.: Tuning the HOMO and LUMO energy levels of organic chromophores for dye sensitized solar cells. J. Org. Chem. **72**(25), 9550–9556 (2007)
13. Chen, R., Yang, X., Tian, H., Wang, X., Hagfeldt, A., Sun, L.: Effect of tetrahydroquinoline dyes structure on the performance of organic dye-sensitized solar cells. Chem. Mater. **19**(16), 4007–4015 (2007)
14. Bredas, J.L., Norton, J.E., Cornil, J., Coropceanu, V.: Molecular understanding of organic solar cells: the challenges. Acc. Chem. Res. **42**(11), 1691–1699 (2009)
15. Labat, F., Ciofini, I., Hratchian, H.P., Frisch, M., Raghavachari, K., Adamo, C.: First principles modeling of eosin-loaded ZnO films: a step toward the understanding of dye-sensitized solar cell performances. J. Am. Chem. Soc. **131**(40), 14290–14298 (2009)
16. Jamorski Jödicke, C., Lüthi, H.P.: Time-dependent density-functional theory investigation of the formation of the charge transfer excited state for a series of aromatic donor-acceptor systems. Part I. J. Chem. Phys. **117**(9), 4146–4156 (2002)
17. Preat, J., Jacquemin, D., Wathelet, V., André, J.M., Perpète, E.A.: TD-DFT investigation of the UV spectra of pyranone derivatives. J. Phys. Chem. A **110**(26), 8144–8150 (2006)
18. Jamorski Jödicke, C., Lüthi, H.P.: Time-dependent density functional theory (TDDFT) study of the excited charge-transfer state formation of a series of aromatic donor-acceptor systems. J. Am. Chem. Soc. **125**(1), 252–264 (2003)
19. Cossi, M., Barone, V.: Time-dependent density functional theory for molecules in liquid solutions. J. Chem. Phys. **115**(10), 4708–4717 (2001)
20. Adamo, C., Barone, V.: A TDDFT study of the electronic spectrum of S-tetrazine in the gas-phase and in aqueous solution. Chem. Phys. Lett. **330**(1–2), 152–160 (2000)
21. Adam, W., Krebs, O.: The nitroso ene reaction: a regioselective and stereoselective allylic nitrogen functionalization of mechanistic delight and synthetic potential. Chem. Rev. **103**(10), 4131–4146 (2003)

22. Baerends, E.J., Ricciardi, G., Rosa, A., van Gisbergen, S.J.A.: A DFT/TDDFT interpretation of the ground and excited states of porphyrin and porphyrazine complexes. Coord. Chem. Rev. **230**(1–2), 5–27 (2002)
23. Casida, M.E.: Jacob's ladder for time-dependent density-functional theory: some rungs on the way to photochemical heaven. In: Low-Lying Potential Energy Surfaces. American Chemical Society, Washington, DC, pp. 199–220 (2009)
24. Bañuelos Prieto, J.: Theoretical study of the ground and excited electronic states of pyrromethene 546 laser dye and related compounds. Chem. Phys. **296**(1), 13–22 (2004)
25. Bertolino, C.A., Ferrari, A.M., Barolo, C., Viscardi, G., Caputo, G., Coluccia, S.: Solvent effect on indocyanine dyes: a computational approach. Chem. Phys. **330**(1–2), 52–59 (2006)
26. Rohrdanz, M.A., Herbert, J.M.: Simultaneous benchmarking of ground- and excited-state properties with long-range-corrected density functional theory. J. Chem. Phys. **129**(3), 034107–10 (2008)
27. Peach, M.J.G., Benfield, P., Helgaker, T., Tozer, D.J.: Excitation energies in density functional theory: an evaluation and a diagnostic test. J. Chem. Phys. **128**(4), 044118–9 (2008)
28. Chiba, B., Tsuneda, T., Hirao, K.: Excited state geometry optimizations by analytical energy gradient of long-range corrected time-dependent density functional theory. J. Chem. Phys. **124**(14), 144106–12 (2006)
29. Kamiya, M., Sekino, H., Tsuneda, T., Hirao, K.: Nonlinear optical property calculations by the long-range-corrected coupled-perturbed Kohn–Sham method. J. Chem. Phys. **122**(23), 234111–11 (2005)
30. Tawada, Y., Tsuneda, T., Yanagisawa, S., Yanai, T., Hirao, K.: A long-range-corrected time-dependent density functional theory. J. Chem. Phys. **120**(18), 8425–8433 (2004)
31. Jacquemin, D., Wathelet, V., Perpète, E.A., Adamo, C.: Extensive TD-DFT benchmark: singlet-excited states of organic molecules. J. Chem. Theory Comput. **5**(9), 2420–2435 (2009)
32. Cherepy, N.J., Smestad, G.P., Grätzel, M., Zhang, J.Z.: Ultrafast electron injection: implications for a photoelectrochemical cell utilizing an anthocyanin dye-sensitized TiO_2 nanocrystalline electrode. J. Phys. Chem. B **101**(45), 9342–9351 (1997)
33. Knorr, F.J., McHale, J.L., Clark, A.E., Marchioro, A., Moser, J.E.: Dynamics of interfacial electron transfer from betanin to nanocrystalline TiO_2: the pursuit of two-electron injection. J. Phys. Chem. C **119**(33), 19030–19041 (2015)
34. Matthews, D., Infelta, P., Grätzel, M.: Calculation of the photocurrent-potential characteristic for regenerative, sensitized semiconductor electrodes. Sol. Energy Mater. Sol. Cells **44**(2), 119–155 (1996)
35. Akın, S., Açıkgöz, S., Gülen, M., Akyürek, C., Sönmezoğlu, S.: Investigation of the photoinduced electron injection processes for natural dye-sensitized solar cells: the impact of anchoring groups. RSC Adv. **6**, 85125–85134 (2016)
36. Jacquemin, D., Perpète, E.A., Scalmani, G., Frisch, M.J., Kobayashi, R., Adamo, C.: Assessment of the efficiency of long-range corrected functionals for some properties of large compounds. J. Chem. Phys. **126**(14), 144105–13 (2007)
37. Marcus, R.: Electron transfer reactions in chemistry: theory and experiment (nobel lecture). Angew. Chem. Int. Ed. **32**, 1111–1121 (1993)
38. Preat, J.: Photoinduced energy-transfer and electron-transfer processes in dye-sensitized solar cells: TDDFT insights for triphenylamine dyes. J. Phys. Chem. C **114**(39), 16716–16725 (2010)
39. Pourtois, G., Beljonne, D., Cornil, J., Ratner, M.A., Brédas, J.L.: Photoinduced electron-transfer processes along molecular wires based on phenylenevinylene oligomers: a quantum-chemical insight. J. Am. Chem. Soc. **124**(16), 4436–4447 (2002)
40. Fitri, A., Benjelloun, A.T., Benzakour, M., Mcharfi, M., Hamidi, M., Bouachrine, M.: Theoretical design of thiazolothiazole-based organic dyes with different electron donors for dye-sensitized solar cells. Spectrochim. Acta A Mol. Biomol. Spectrosc. **132**(C), 232–238 (2014)
41. Ding, W.L., Wang, D.M., Geng, Z.Y., Zhao, X.L., Xu, W.B.: Density functional theory characterization and verification of high-performance indoline dyes with D-A-π-A architecture for dye-sensitized solar cells. Dyes Pigments **98**(1), 125–135 (2013)
42. Hsu, C.P.: The electronic couplings in electron transfer and excitation energy transfer. Acc. Chem. Res. **42**(4), 509–518 (2009)
43. Katoh, R., Furube, A., Yoshihara, T., Hara, K., Fujihashi, G., Takano, S., Murata, S., Arakawa, H., Tachiya, M.: Efficiencies of electron injection from excited N3 dye into nanocrystalline semiconductor (ZrO_2, TiO_2, ZnO, Nb_2O_5, SnO_2, In_2O_3) films. J. Phys. Chem. B **108**(15), 4818–4822 (2004)
44. Zhang, C.R., Liu, L., Zhe, J.W., Jin, N.Z., Ma, Y., Yuan, L.H., Zhang, M.L., Wu, Y.Z., Liu, Z.J., Chen, H.S.: The role of the conjugate bridge in electronic structures and related properties of tetrahydroquinoline for dye sensitized solar cells. Int. J. Mol. Sci. **14**(3), 5461–5481 (2013)
45. Fan, W.: Incorporation of thiadiazole derivatives as π-spacer to construct efficient metal-free organic dye sensitizers for dye-sensitized solar cells: a theoretical study. Commun. Comput. Chem. **1**, 152–170 (2013)
46. Tian, H., Yang, X., Pan, J., Chen, R., Liu, M., Zhang, Q., Hagfeldt, A., Sun, L.: A triphenylamine dye model for the study of intramolecular energy transfer and charge transfer in dye-sensitized solar cells. Adv. Funct. Mater. **18**(21), 3461–3468 (2008)
47. Zhang, Z., Zou, L., Ren, A., Liu, Y., Feng, J., Sun, C.: Theoretical studies on the electronic structures and optical properties of star-shaped triazatruxene/heterofluorene copolymers. Dyes Pigments **96**, 349–363 (2013)
48. Sang-aroon, W., Saekow, S., Amornkitbamrung, V.: Density functional theory study on the electronic structure of monascus dyes as photosensitizer for dye-sensitized solar cells. J. Photochem. Photobiol. A Chem. **236**, 35–40 (2012)
49. Frisch, M.J., Trucks, G.W., Schlegel, H.B., Scuseria, G.E., Robb, M.A., Cheeseman, J.R., Scalmani, G., Barone, V., Mennucci, B., Petersson, G.A., Nakatsuji, H., Caricato, M., Li, X., Hratchian, H.P., Izmaylov, A.F., Bloino, J., Zheng, G., Sonnenberg, J.L., Hada, M., Ehara, M., Toyota, K., Fukuda, R., Hasegawa, J., Ishida, M., Nakajima, T., Honda, Y., Kitao, O., Nakai, H., Vreven, T., Montgomery, Jr., J.A., Peralta, J.E., Ogliaro, F., Bearpark, M., Heyd, J.J., Brothers, E., Kudin, K.N., Staroverov, V.N., Kobayashi, R., Normand, J., Raghavachari, K., Rendell, A., Burant, J.C., Iyengar, S.S., Tomasi, J., Cossi, M., Rega, N., Millam, J.M., Klene, M., Knox, J.E., Cross, J.B., Bakken, V., Adamo, C., Jaramillo, J., Gomperts, R., Stratmann, R.E., Yazyev, O., Austin, A.J., Cammi, R., Pomelli, C., Ochterski, J.W., Martin, R.L., Morokuma, K., Zakrzewski, V.G., Voth, G.A., Salvador, P., Dannenberg, J.J., Dapprich, S., Daniels, A.D., Farkas, O., Foresman, J.B., Ortiz, J.V., Cioslowski, J., Fox, D.J.: Gaussian 09 Revision E.01, Gaussian Inc., Wallingford CT (2009)
50. Peverati, R., Truhlar, D.G.: Screened-exchange density functionals with broad accuracy for chemistry and solid-state physics. Phys. Chem. Chem. Phys. **14**(47), 16187–16191 (2012)
51. Krishnan, R., Binkley, J.S., Seeger, R., Pople, J.A.: Self-consistent molecular orbital methods. XX. A basis set for correlated wave functions. J. Chem. Phys. **72**(1), 650–654 (1980)
52. Kim, B., Chung, K., Kim, J.: Molecular design principle of all-organic dyes for dye-sensitized solar cells. Chem. A Eur. J. **19**, 5220–5230 (2013)
53. Zhu, W., Wu, Y., Wang, S., Li, W., Li, X., Chen, J., Wang, Z.S., Tian, H.: Organic D-A-π-A solar cell sensitizers with improved

stability and spectral response. Adv. Funct. Mater. **21**(4), 756–763 (2011)
54. Lakshmanakumar, M., Sriram, S., Balamurugan, D.: Performance analysis of TiO_2-flavylium compound-based dye-sensitized solar cell (DSSC): a DFT-TDDFT approach. J. Comput. Electron. **17**, 1143–1152 (2018)
55. Jin, X., Li, D., Sun, L., Wang, C.L., Bai, F.Q.: Theoretical design of porphyrin sensitizers with different acceptors for application in dye-sensitized solar cells. RSC Adv. **8**, 19804–19810 (2018)